Review Paper

A review of high-performance MEMS sensors for resource exploration and geophysical applications

Hua-Feng Liu [a], Zhi-Cai Luo [a, b], Zhong-Kun Hu [a], Shan-Qing Yang [a, c, d], Liang-Cheng Tu [a, c, d, *], Ze-Bing Zhou [a, **], Michael Kraft [e]

[a] National Precise Gravity Measurement Facility (PGMF) and School of Physics, Huazhong University of Science and Technology, Wuhan, Hubei, 430074, China
[b] Institute of Geophysics, Huazhong University of Science and Technology, Wuhan, Hubei, 430074, China
[c] TianQin Research Center for Gravitational Physics and School of Physics and Astronomy, Sun Yat-sen University (Zhuhai Campus), Zhuhai, Guangdong, 519082, China
[d] Nanchang Research Institute, Sun Yat-sen University, Nanchang, Jiangxi, 330099, China
[e] ESAT-MNS, University of Leuven, Leuven, Belgium

ARTICLE INFO

ABSTRACT

MEMS sensors have the advantages of small volume, lightweight, and low cost, therefore, have been widely used in the fields of consumer electronics, industry, health, defence, and aerospace. With their ever-improving performance, MEMS sensors have also started to be used in resource exploration and geophysical applications. However, the requirements of high-precision MEMS sensors for geophysical applications have not been specified in detail. Therefore, this paper systematically analyzes the requirements of high-performance MEMS sensors for prospecting and geophysical applications, including seismic surveillance, Earth tide, volcanic activity monitoring for natural disasters; seismic, gravity, and magnetic resource prospecting; drilling process monitoring and local gravity measurement for gravity aided navigation. Focusing on the above applications, this paper summarizes the state-of-the-art of research on high-performance MEMS sensors for resource exploration and geophysical applications. Several off-the-shelf MEMS sensors have been used for earthquake monitoring, seismic exploration and drilling process monitoring, and a range of MEMS research prototype sensors have successfully been employed for Earth tides measurement and are promising to be used for gravity exploration. MEMS magnetometers should have a lower noise floor to meet the demand for magnetic exploration. MEMS gravity gradiometers are still under early development and will not be deployable in short-term. High-performance MEMS sensors hold the advantages of low-cost, high integration, and capability of working in extreme environments; therefore, they are likely to gradually replace some conventional geophysical instruments in some application areas.

1. Introduction

Micro ElectroMechanical Systems (MEMS) refer to micro devices or systems which combine microstructures, micro-transducers, and micro-actuators with signal processing and control circuits. Their fabrication technology is inherited from integrated circuits (IC) with the critical dimensions in the micrometer to millimeter range. MEMS sensors are sensors manufactured by microfabrication technology using silicon, quartz, metal or other semiconductor materials for sensing physical or chemical quantities. Compared with conventional sensors, MEMS sensors have the inherent advantages of being compact, lightweight, integratable, and can be batch fabricated, thus being low-cost. Therefore, in the past thirty years, they have been widely used in many emerging areas and are replacing conventional sensors in low-to-medium end application fields. In the fields of consumer electronics and automobiles, low-cost MEMS sensors have been widely adapted in

* Corresponding author. National Precise Gravity Measurement Facility (PGMF) and School of Physics, Huazhong University of Science and Technology, Wuhan, Hubei, 430074, China.
** Corresponding author.
E-mail addresses: tuliangch@sysu.edu.cn (L.-C. Tu), zbzhou@hust.edu.cn (Z.-B. Zhou).

smartphones, gaming consoles, air-bag deployment and vehicle stabilization systems, as well as, positioning and navigation in buildings, basements and tunnels. In addition, MEMS sensors have also been used in biomedical and industrial fields. With the fast development of the MEMS technology, high-end MEMS sensors have been developed for defence and aerospace applications, including tactical-grade inertial navigation, orbital perturbation measurement under a microgravity environment. Over the last decade, high-precision MEMS sensors have emerged in geophysical and resource search fields, such as MEMS seismic sensors for oil exploration. To date, however, there is no systematic analysis and summary for geophysical and exploration application requirements. In this review article, therefore, we analyze the requirements for high-precision MEMS sensors, describe the state-of-the-art of MEMS sensors for geophysical applications, and present an outlook for future developments.

2. Sensor requirements for resource exploration and geophysical applications

2.1. Earthquake monitoring

Earthquake is the phenomenon of a series of vibrations induced in the Earth's crust by the abrupt rupture and rebound of rocks in which elastic strain has been slowly accumulating. Seismic sensors are used to monitor earthquakes for deducing their location, depth, magnitude, and seismic intensity. The collected data can be used to understand the evolution process of geological disasters and reduce the impact of natural hazards. In addition, short-time earthquake forecasting can be implemented by using the time lag between the faster P-wave and the more destructive surface wave so that loss of life and personal injury can be reduced.

Since Zhang Heng invented the seismic orientation indicator in ancient China, seismic sensors have become gradually mature. According to the detectable seismic intensity, seismic sensors can be categorized as strong-motion and weak-motion seismometers. The self-noise level of weak-motion seismometers is generally lower than 1 ng/$\sqrt{Hz}$, such as the commercial macroscopic devices CMG-3T from Guralp and Trillium 120 from Nanometrics. Several high-end seismometers have an even lower noise floor than the Earth's new low noise model (NLNM), such as the model STS 2.5 from Kinemetrics. By contrast, the strong-motion seismometers generally have a noise floor of above 1 µg/$\sqrt{Hz}$, such as some high-resolution force-balance accelerometers like the models CMG-5U from Guralp and Epi-sensor from Kinemetrics. In addition, due to the equivalence principle of inertial acceleration and gravitational acceleration, atmosphere and other effects induced tilt cannot be distinguished by a single seismic sensor; therefore, tilt-meters or angular accelerometers are required to measure the tilt angle and then compensate to minimize the sensitivity error. Since the frequency of earthquake signals is generally between 8.3 mHz (120 s) and 50 Hz, the bandwidth of the seismometers and angular accelerometers are required to cover this range.

2.2. Seismic exploration

Seismic exploration is an essential method for gas and oil exploration and has also been widely used in geological surveys and crust studies. Seismic methods depend upon velocities of acoustic energy propagation in Earth materials. This method includes the generation of a short pulse of seismic energy and subsequent recordings of the arrival of the seismic pulse at distant locations. An explosion or the impact of a mass on the Earth's surface provides the energy detected by sensitive geophones or seismometers, which contain electronic amplifiers and a suitable recorder. Wave theories of travel time, reflection, absorption, diffusion, and refraction are employed for seismic interpretation, from which it is possible to infer the properties of underground rock formations, and thus the location of oil and gas resources.

Geophones are much cheaper than seismometers, therefore geophones are more likely to be used in arrays for large-area seismic exploration. Before MEMS technology was used in seismology, there were evident differences between geophones and seismometers. Conventional geophones specifically refer to coil-magnets-based passive components which respond to the ground motion above their natural frequency, which is in the range of 1−60 Hz. Compared with geophones, seismometers are more suitable for extremely small and slow ground motion detection, typically from 0.01 to 50 Hz, which includes the frequency range below their natural frequency. Emerging MEMS-based geophones are basically high-sensitive MEMS accelerometers that can cover a large frequency band from DC to 500 Hz; therefore, the boundary between geophones and seismometers has become somewhat blurred (Hou et al., 2021). Conventional geophones have a current flow out from the coil due to the relative motion between the coil and magnets. Thus they do not require active driving electronics for a signal pickoff, which is required by both MEMS geophones and seismometers in contrast. Thus, conventional geophones are passive while MEMS geophones and seismometers are active. In addition, conventional geophones and seismometers are velocity meters with a flat velocity frequency response and band-pass characteristic, while MEMS geophones are accelerometers with a flat acceleration frequency response and low-pass characteristic. Therefore, MEMS geophones tend to have a better low-frequency response than conventional geophones. The photos of typical geophone, seismometer and MEMS seismic sensor are shown in Fig. 1.

2.3. Gravity exploration

The gravity method is a geophysical exploration method to determine the physical properties and structures of the Earth; others being from seismic, magnetic, and electrical methods. It is based on the measurement of changes in the gravity field caused by variations of density within the subsurface. In other words, a gravity anomaly, which the gravity method observes and studies, is due to a local density difference of the mass to the wider area and affects the local gravity field (Hinze et al., 2013). The gravity method has been used in the regional characterization of Earth for determining the crust architecture and identifying regions for resource explorations.

Gravimeters are commonly used to measure gravity acceleration in the gravity method. According to the different measurement methods of gravity acceleration, gravimeters are divided into absolute gravimeters and relative gravimeters. Absolute gravimeters can accurately measure the gravity acceleration of an object by measuring the distance and time of its free fall. Typical commercial absolute gravimeters include FG5 and A10 from Micro-g LaCoste, and AQG from Muquans, etc. Relative gravimeters measure the gravity acceleration by measuring the change of elongation of a spring or the change of displacement due to mass sag. Typical commercial relative gravimeters include Scintrex CG-6, GWR iGrav, gPhone, and the airborne GT-2A. The gravity acceleration is the first derivative of the gravitational potential. The gradient of the gravity acceleration with respect to the spatial location is called the gravity gradient, which is also the second derivative of the gravitational potential. Compared with gravity measurements, gravity gradient measurement has a higher spatial resolution and can infer details of the field source body; hence it has a wider application potential. A gravity gradiometer is the instrument used to measure the gravity
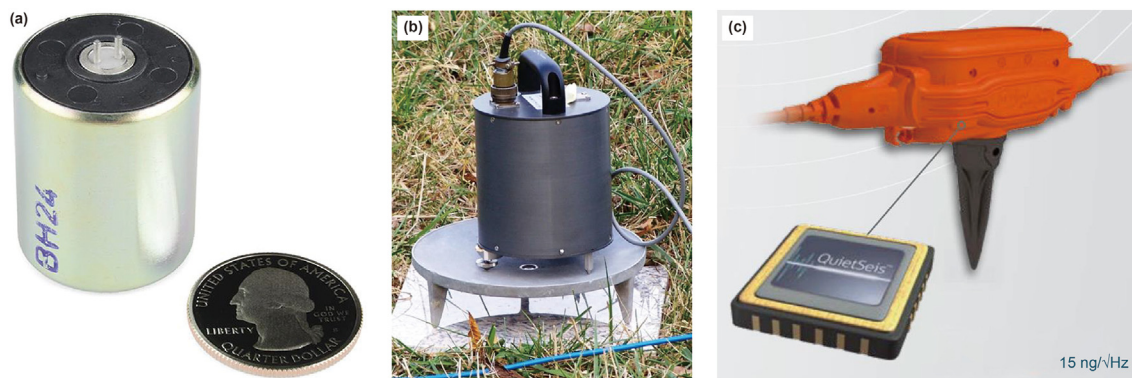
Fig. 1. Photos of commercial geophones, conventional seismometers, and MEMS seismic sensors. (a) Geophone; (b) seismometer; (c) MEMS seismic sensor from Sercel.

gradient tensor elements. Currently, the only practical gravity gradiometers used for gravity exploration in the world are the rotary-accelerometer-based gravity gradiometers developed by Lockheed Martin Ltd. The developmental versions were divided into the partial tensor gravity gradiometer (BHP's Falcon system) and the full tensors gravity gradiometer (Bell Geospace's AIR-FTG system) (Dransfield and Christensen, 2013).

2.4. Magnetic exploration

Earth's geomagnetic field is generated due to the liquid outer core of the Earth, the magnetic rocks of Earth's crust, and the solar activities induced magnetic field (Hinze et al., 2013). Magnetic exploration is a geophysical research method developed earlier and has been widely used to obtain the spatial distribution and composition of the detection area by monitoring and analyzing magnetic anomalies and magnetic differences in the target area by magnetic sensors. It has been proven by engineering applications that magnetic exploration has the advantages of high efficiency, low cost, and wide work range; therefore, it has become the main geophysical exploration method (Hinze et al., 2013). In addition, the data by continuously monitoring the changes of geomagnetic fields can be used for geomagnetic scientific research, earthquake prediction research, and even social application research.

With the development of the marine survey, resource exploitation, and the development of magnetic sensor technologies, magnetic exploration has gradually evolved from single-point field measurement to three-component vector measurement and subsequent to magnetic gradient measurement. Therefore, high-performance magnetic sensors are required. According to the working principle, magnetic sensors can be categorized as fluxgate, induction, SQUID, proton, atomic, and MEMS magnetometers, which include micro fluxgate, Hall, magneto-resistance, and resonant magnetometers. The required measurement range of the magnetometers for resource exploration and geophysical applications is between 10 pT and 100 μT (Ripka, 2021).

2.5. Drilling process monitoring

During an oil and gas drilling process, the drill string deforms due to the interaction between the drill string and the borehole wall; therefore, the drill head interacts with rocks in complex vibration patterns. Drilling tool vibration mainly can be classified as torsional, axial, and transverse vibrations. The actual drilling process usually comprises coupling of those three kinds of vibrations. Real-time monitoring of drilling tool vibrations can help to understand the working condition of the drilling tool and prevent drilling tool accidents.

Axial and transverse vibrations can be measured with accelerometers, while torsional vibrations can be measured by gyroscopes or angular accelerometers. The angular displacement can be derived by either integrating the angular rate or integrating the angular acceleration twice. However, any DC component of rates or accelerations will result in displacement errors and the errors accumulate. In this case, gyroscopes provide intrinsically fewer displacement errors than angular accelerometers; therefore, gyroscopes are largely used in positioning and navigation applications. For gyroscopes, angular accelerations have to be derived by differentiating the measured angular rates over the sampling periods. In contrast, angular accelerometers directly measure angular accelerations. Hence, angular accelerometers have a faster response for angular vibrations or shocks, so they are largely used in some specific fields, such as the Jewell ASB Series (Jewell-ASB), Endevco 7302BM4 (Endevco-7392BM4), and Kistler 8838 (Kistler-8838). Although these conventional angular accelerometers can achieve lower fundamental frequencies to obtain better sensitivity or response to low-frequency signals; however, for large-scale deployments, cost and efficiency must be considered.

2.6. Earth tides and volcanic activity monitoring

Due to the gravitational force from the sun, the moon, and other planets, tidal phenomena occur in rivers, lakes, and seas. For the same reason, the solid Earth also exhibits periodic deformation phenomenon, usually referred to as Earth tides (Cochran et al., 2004). The tidal deformation of the Earth is closely related to the physical characteristics of the medium such as density, so the observation and study of the Earth tides is an important basis for understanding the structure and changes of the Earth's interior. A volcanic eruption is the most intense display of the release of the Earth's internal heat energy; an eruption will produce a large amount of ash and lava flow, which can be devastating. Gravity measurement around a volcano can be used to monitor volcanic activity such as magma ejection; therefore, gravity variation data may be used for forecasting volcanic eruption (Hinze et al., 2013).

Both Earth tide and volcanic activity produce gravity acceleration varying with time at the same location (Kasahara, 2002). Long-term monitoring of local time-varying gravity fields by absolute or relative gravimeters can further understand Earth's internal structure and forecast natural disasters. Absolute gravimeters are far more expensive than relative gravimeters; therefore, the latter is commonly used. The frequency of gravity time-varying signals such as Earth tide is about 10^{-5} Hz or even lower, so high long-term stability of relative gravimeters is required.

2.7. Gravity aided navigation

Gravity-aided navigation is a kind of navigation and positioning technology that uses gravimeters or gravity gradiometers to measure the characteristics of the regional gravity field in real time and conduct tracking and matching with a known Earth gravity field map to determine the current location. Gravity-aided navigation is mainly used to correct the accumulated errors of inertial navigation systems over time. The integrated navigation system with both inertial navigation and gravity-aided navigation has the advantages of high precision, passive, and no Global Navigation Satellite System (GNSS) requirement; therefore, it is promising to meet long-term autonomous navigation requirements (Affleck and Jircitano, 1990).

Gravity-aided navigation requires gravity field mapping, high-precision gravity real-time measurement instruments, and gravity field matching software. As reported so far, only the US has the ability of long-term underwater navigation with gravity-aided navigation technology (Wang et al., 2016). A high-precision gravity real-time measurement instrument is the bottleneck of gravity-aided navigation technology, and the requirement for high precision accelerometers with a large dynamic range as the core unit of gravity measurement is the key problem to be solved.

3. Research status of related MEMS sensors

With the fast development of MEMS technology in recent years, more and more high-precision MEMS sensors, including MEMS seismometers, tiltmeters, angular accelerometers, magnetometers, relative gravimeters, and gravity gradiometers, have been used or show promise to be used in the field of geophysics and resource exploration. The advent of these high-precision MEMS sensors is expected to provide an effective solution for geophysical applications with low-cost requirements, volume and weight constraints, or for harsh environments.

3.1. MEMS accelerometers and gravimeters

3.1.1. Principles and classification

MEMS accelerometers measure translational accelerations for one or several axes. The basic working principle of most micromachined accelerometers is based on the spring-mass system, in which a proof mass is suspended by compliant beams anchored to a fixed frame (Beeby et al., 2004). In a second-order model, a damper is also included to control dynamic vibration. Accelerometers are generally characterized by their resolution, sensitivity (scale factor), dynamic range, working bandwidth, non-linearity, offset, drift, off-axis sensitivity, and shock survival (Yazdi et al., 1998). These parameters depend on both the mechanical suspension design and the displacement or force measurement methods. Based on the displacement sensing mechanisms, MEMS accelerometers can be categorized by different types of transduction method: capacitive (Abdolvand et al., 2007), piezoelectric (Hindrichsen et al., 2009) and piezoresistive (Haris and Qu, 2010) accelerometers, and also other methods such as tunneling (Liu and Kenny, 2001), resonant (Zou and Seshia, 2015), thermal (Chen and Shen, 2008), optical (Littler et al., 2010), and electromagnetic (Phan et al., 2008) sensors. Based on the working mode, MEMS accelerometers can be categorized as open-loop and closed-loop systems, depending on whether there is a force feedback control loop.

For the open-loop system, the performance of an accelerometer is mainly determined by its mechanical structure so that the working bandwidth is limited by its natural frequency, however, the open-loop circuit is simple and stable. A closed-loop system can improve the overall linearity, dynamic range and bandwidth of an accelerometer, which is attributed to the force feedback control

maintaining the proof mass near to its null position.

The essential requirements of the MEMS accelerometers are highly application dependent. Fig. 2 depicts the corresponding work range and bandwidth requirements of MEMS accelerometers for different applications. Although the information in the overview chart may not be very accurate or complete, the chart can still give readers an overview of the application areas for MEMS accelerometers. Currently, MEMS accelerometers for most applications have been successfully commercialized. Manufacturers typically concentrate on cost, power consumption and reliability of the accelerometers, while the resolution (noise floor) is not regarded as the bottleneck. However, for seismic-grade MEMS accelerometers, high-resolution (low noise floor) is still a major challenge and therefore many technologies are still under development, and only a few have been commercialized.

In addition, MEMS relative gravimeters, as a kind of special MEMS accelerometers, have the ultimate performance of ultra-sensitive, ultra-stable (low drift), and ultra-low frequency response (generally for 10^{-5} Hz). So far, there are a few seismic-grade MEMS accelerometers that can meet the above-mentioned requirements.

3.1.2. MEMS seismic-grade accelerometers

Seismic-grade accelerometers require a very low noise floor, i.e. less than 1 $\mu g/\sqrt{Hz}$, and need to be very sensitive within a measurement range of a few times the Earth's gravitational acceleration. For seismology applications, an accelerometer is used to record seismic signals, performing as a seismometer. The natural period of a seismometer, or the reciprocal of natural frequency, is an important factor in determining what the seismometer actually records. For a long-period (LP) seismometer, with a resonant frequency ω_0 much smaller than the seismic waves ($\omega_0 \ll \omega$), the phase-lag between the seismometer and the ground motion is zero. In this case, the displacement of the LP seismometer proof mass is proportional to the ground displacement, so that the LP seismometer can also be used as a displacement sensor. LP seismometers are designed to record seismic signals with frequencies of 0.01–0.1 Hz. A short-period (SP) seismometer has a natural frequency that is much larger than most frequencies in the seismic waves ($\omega_0 \gg \omega$), so that the displacement of the SP proof mass is proportional to the acceleration of the ground. Hence, SP seismometers can also perform as accelerometers to measure the ground vibrations with frequencies of 0.1–10 Hz. Both LP and SP seismometers have a narrow bandwidth. In contrast, broadband
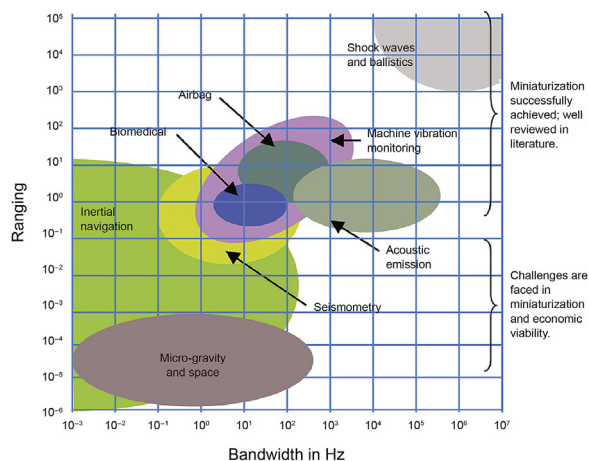

Fig. 2. Working range and bandwidth of MEMS accelerometers for various applications (Krishnan et al., 2007).

(BB) seismometers can record seismic signals with frequencies of 0.01–10 Hz, obtaining more valuable information than that from LP or SP seismometers individually or in combination (William, 2007). Based on the classification, the seismic-grade MEMS accelerometers are possible to be used as SP or BB seismometers.

A comparison of performance requirements of MEMS accelerometers for seismology applications is listed in Table 1 in terms of noise floor, bandwidth, peak acceleration, and dynamic range, based on the literature (Merchant, 2009). Depending on the resolution, accelerometers with a noise floor of around 1 μg/√Hz can only detect strong motions of seismic activities. In order to record weak motions, the noise floor of accelerometers has to be lower than 1 ng/√Hz (Merchant, 2009). It is necessary to figure out how far current MEMS accelerometers are away from performing as seismometers. Most commercialized seismic-grade MEMS accelerometers with a noise floor of below 1 μg/√Hz are based on capacitive, optical, and piezoelectric displacement transducers. There are also some examples of resonant, electrochemical and tunneling MEMS accelerometers for seismic applications. A broad overview of state-of-the-art seismic-grade MEMS accelerometers, compared with three conventional seismometers, is shown in Fig. 3, in terms of the demonstrated minimum acceleration noise floor and the achieved maximum bandwidth. It should be mentioned that the noise floor usually does not correspond to the value at the maximum bandwidth, rather it is the minimum value in the operating bandwidth, generally, at much lower frequencies than the maximum bandwidth value.

Commercialized seismic-grade MEMS accelerometers are mainly based on capacitive, optical, and piezoelectric transduction mechanisms. Off-the-shelf capacitive seismic-grade MEMS accelerometers are from Colibrys, INOVA, MT Microsystems, and Sercel, which are all electrostatic force feedback controlled closed-loop MEMS accelerometers. Model SF1500 (Laine and Mougenot, 2014) from Colibrys (now part of the Safran Group) has a noise floor of 300 ng/√Hz with a bandwidth of DC to 1500 Hz in a working range of ±3 g. The digital triaxial model VectorSeis ML21 (Vectorseis-ML21) from INOVA, providing a noise floor of 40 ng/√Hz with a bandwidth of 3 Hz–375 Hz in a working range of ±0.3 g. Model MSV3000-2 (MTMicrosystems, MSV3000-2) from MT Microsystems in China can provide a noise floor of 200 ng/√Hz with a bandwidth of DC to 250 Hz in a working range of ±2 g. DSU-508 (Laine and Mougenot, 2014) from the French company Sercel can have a noise floor of 12 ng/√Hz with a bandwidth of DC to 800 Hz in a working range of ±0.5 g. Colibrys SF1500 and MT MSV3000-2 have suspended their production. The optical MEMS seismometer Model 203-60 from Silicon Audio adopts optical interferometric displacement sensing and electromagnetic force feedback, with a minimum noise level of 0.5 ng/√Hz@10 Hz, a dynamic range of 172 dB@1 Hz, a clip level of ±0.5 g and a flat acceleration output in the range of 0.005–1500 Hz (Silicon Audio-203). Piezoelectric effect-based acceleration sensing is a mature technology. Although the off-of-shelf piezoelectric seismic-grade accelerometers are not strictly MEMS, they have comparatively small dimensions, as well as some MEMS capacitive accelerometers. PCB Piezotronics Model
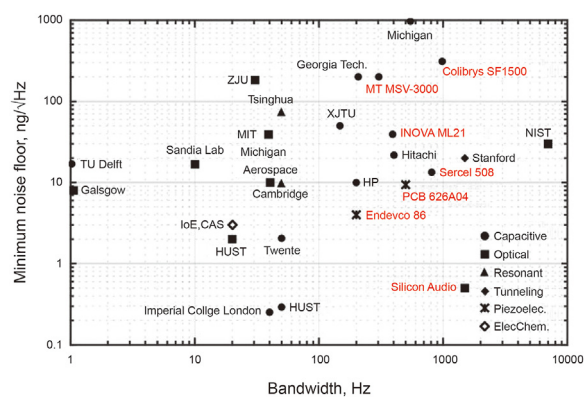

Fig. 3. State-of-the-art seismic-grade MEMS accelerometers in terms of the maximum bandwidth and their lowest acceleration noise in the bandwidth (off-the-shelf products in red).

626A04 (PCB-626A04) seismic accelerometers have a size of 57.2 mm in diameter with a height of 53.3 mm and a noise floor of 10 ng/√Hz above 100 Hz. Endevco, a division of the Meggitt group, has the Model 86 accelerometer with a similar size as the counterpart from PCB Piezotronics. Model 86 (Endevco-86) has a noise floor of 4 ng/√Hz above 100 Hz. Both seismic-grade piezoelectric accelerometers have the maximum acceleration range of ±0.5 g, a frequency response from the order of 10 mHz to a few hundred Hertz. Several commercial seismic-grade MEMS accelerometers are shown in Fig. 4.

Most seismic-grade MEMS accelerometers are still being researched, and concentrate on capacitive, optical, and resonant transduction mechanisms. Research work for capacitive seismic-grade accelerometers can be categorized as gap-variation and area-variation approaches, as shown in Fig. 5. Gap-variation designs improve the sensor performance by reducing the sensing gap and increasing the proof mass. Researchers from Georgia Institute of Technology (Abdolvand et al., 2007) used a surface and bulk combined process to fabricate the bulky mass of a whole-wafer thickness of 475 μm and a sacrificial oxide layer to form a sensing gap of 1.5 μm, achieving a noise floor of 1080 ng/√Hz. While researchers from University of Michigan (Chae et al., 2005) used an SOI wafer attached with an extra mass and a sensing gap of around 4 μm, providing a noise floor of 213 ng/√Hz at 2 Hz. Hitachi from Japan developed a gap-variation MEMS capacitive accelerometer with a noise floor of 22 ng/√Hz, a working range of 0.55 g, and a bandwidth of 400 Hz (Furubayashi et al., 2019). The low noise floor is obtained by using an asymmetric teeter-totter structure for lowering Brownian noise and digital noise reduction technology for suppressing electrical noise.

Unlike gap-variation counterparts, high-resolution area-variation accelerometer designs improve the noise performance using the most volume of each die as seismic mass and plate biplanar electrodes arrays to increase the capacitance-to-acceleration sensitivity. Hewlett-Packard (Milligan et al., 2011) developed an open-loop lateral sensing MEMS accelerometer, providing a noise floor of 10 ng/√Hz, a working range of 80 mg and a bandwidth of 200 Hz. Pike et al. (2014) from Imperial College London developed the most sensitive silicon accelerometer to date as a contribution to NASA's InSight Mars mission to investigate Martian seismic activities (Pike et al., 2014; Lognonné et al., 2019). This seismic accelerometer has a demonstrated noise floor of 0.25 ng/√Hz at 1 Hz and below 1 ng/√Hz between 0.1 Hz and 10 Hz. With the electromagnetic force feedback control, the bandwidth is up to 40 Hz (Pike et al., 2016, 2018). In addition, a research group of Huazhong University of Science and Technology (HUST) has also developed an

Table 1
Sensor types for seismology applications.

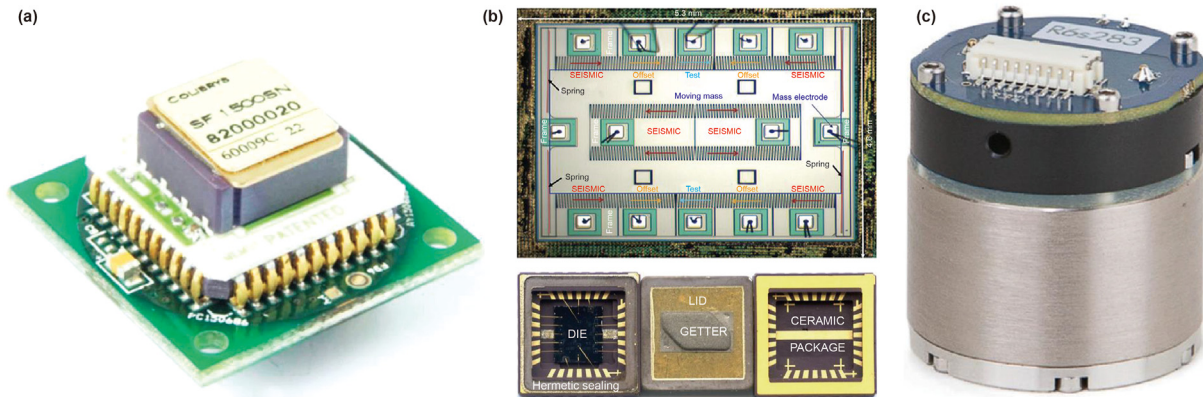| Parameters	Strong motion	Weak motion
Noise floor	<1 μg/√Hz	<1 ng/√Hz
Bandwidth	>100 Hz	SP: 0.1 Hz–10 Hz
		LP: 0.01 Hz–0.1 Hz
		BB: 0.01 Hz–10 Hz
Peak acceleration	1–3 g	<0.25 g
Dynamic range	~100 dB	>120 dB

Fig. 4. Commercialized seismic-grade MEMS accelerometers. (a) Colibrys SF1500; (b) Sercel DSU 508; (c) Silicon Audio.
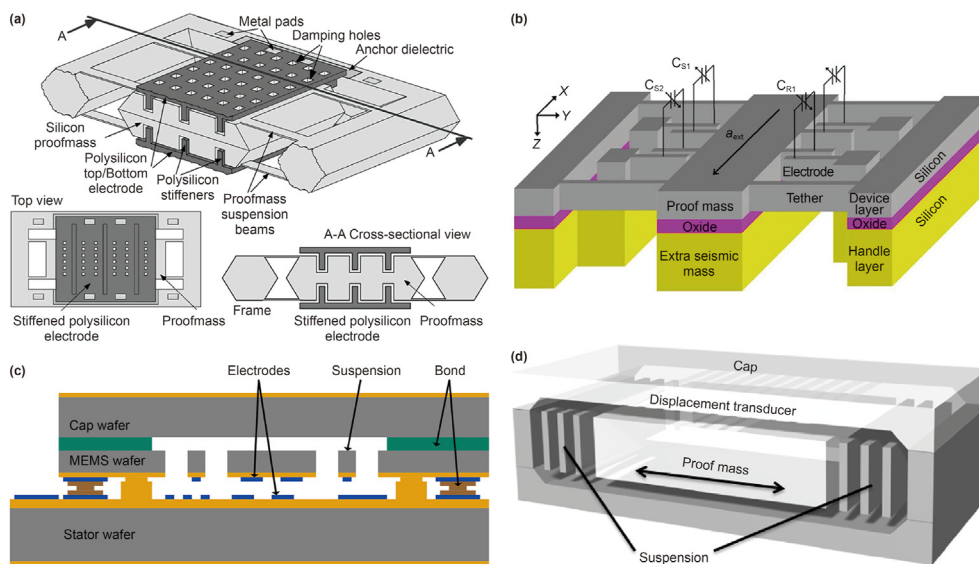

Fig. 5. Seismic-grade MEMS capacitive accelerometers. (a) Uni. of Michigan, gap-variation (Abdolvand et al., 2007); (b) Georgia Tech., gap-variation (Chae et al., 2005); (c) Hewlett-Packard, area-variation (Milligan et al., 2011); (d) Imperial College, area-variation (Pike et al., 2009).

area-variation-based capacitive MEMS seismometer with a noise floor of 0.3 ng/$\sqrt{Hz}$ at 1 Hz and a bandwidth of 50 Hz (Wang et al., 2019).

At present, the most high-sensitivity MEMS accelerometers are based on area-variation capacitive sensing mechanisms with a large inertial mass. An emerging approach is based on non-linear springs which may have the potential to achieve both high-sensitivity and small-size. University of Twente (Boom et al., 2017) reported a seismic-grade MEMS accelerometer using the geometric anti-spring non-linear suspension system, obtaining a noise floor of 2 ng/$\sqrt{Hz}$ and a demonstrated bandwidth of 50 Hz. The stiffness of the curved leaf springs shown in Fig. 6a was reduced by a factor of 26 by an anti-reverse structure pre-loading mechanism. In addition, the stiffness reduction is independent of the proof-mass position and consumes no power due to its purely mechanical realization. In contrast, the MEMS accelerometer developed by TU Delft (El Mansouri et al., 2019), as shown in Fig. 6b, utilized the gravitational force to achieve pre-loading for a lower stiffness; however, the proof-mass position changed after the force loading. This sensor has a noise floor of 17 ng/$\sqrt{Hz}$ and a bandwidth of 1 Hz which is limited by its resonant frequency. The MEMS accelerometer developed by Xi'an Jiao Tong University (XJTU) (Zhang et al., 2019) as shown in Fig. 6c mainly used

the electrostatic force to preload anti-springs, yielding a noise floor of 50 ng/$\sqrt{Hz}$ and a bandwidth of 158 Hz. However, due to the electrostatic force loading, the mechanical properties coupled with the voltage fluctuation; therefore, the stability of accelerometers based on the electrostatic pre-loading mechanism may highly rely on the voltage stability.

Optical displacement sensing is another approach for implementing seismic-grade MEMS accelerometers. Fig. 7 shows the interferometric and grating diffraction-based optical MEMS accelerometers. Sandia National Laboratory (Krishnamoorthy et al., 2008) developed an in-plane sub-wavelength nano-grating accelerometer with an ultrasensitive optical displacement transducer (50 fm/$\sqrt{Hz}$@0.01Hz), providing a noise floor of 17 ng/$\sqrt{Hz}$@1Hz. Zhejiang University (ZJU) reported a grating interferometry-based out-of-plane MEMS accelerometer with a noise floor of 185.6 ng/$\sqrt{Hz}$ and a bandwidth of 30 Hz. MIT (Loh et al., 2002) developed an interferometric MEMS accelerometer with the proof mass and the integrated inter-digital position detector fabricated by a two-mask process. The proposed accelerometer has a noise floor of 40 ng/$\sqrt{Hz}$ and a bandwidth of 40 Hz. HUST (Qu et al., 2020) reported a Fabry—Pérot interference-based MEMS accelerometer with a noise floor of 2.4 ng/$\sqrt{Hz}$@10Hz and a bandwidth of 20 Hz.
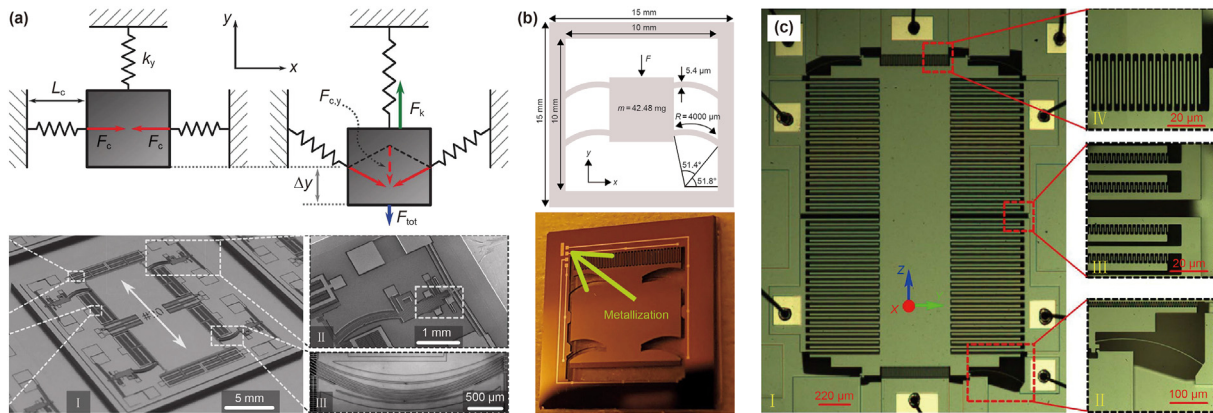
Fig. 6. MEMS accelerometers based on anti-spring non-linear suspension systems. (a) Uni. of Twente (Boom et al., 2017); (b) TU Delft (El Mansouri et al., 2019); (c) XJTU (Zhang et al., 2019).
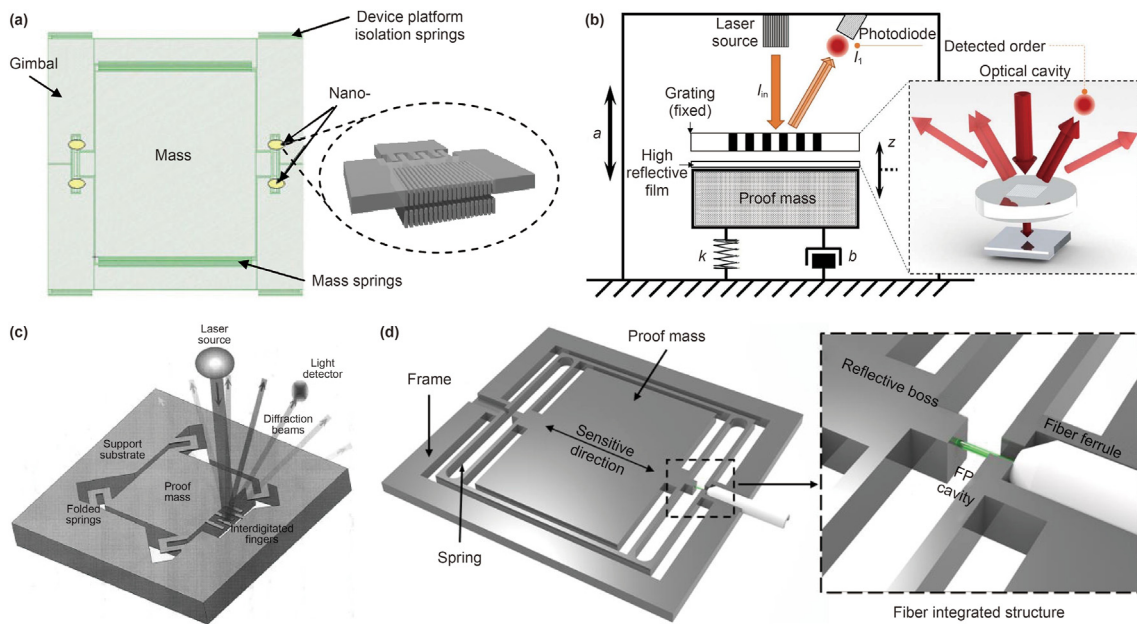

Fig. 7. Optical interferometric and grating diffraction-based MEMS accelerometers. (a) Sandia Lab (Krishnamoorthy et al., 2007); (b) Zhejiang Uni. (Lu et al., 2017); (c) MIT (Loh et al., 2002) (d) HUST (Qu et al., 2020).

The above-mentioned optical MEMS accelerometers utilize conventional optical effects, where the optical force can be neglected compared with the mechanical forces. However, in terms of cavity optomechanical effects, the optical resonance boosts the optical field thousands of times; therefore, the interaction between optical radiation pressure and mechanical structure is significantly amplified in optical micro-cavities. The optical field is very sensitive to mechanical motion, which therefore can be used for acceleration and displacement sensing (Metcalfe, 2014). The optomechanical cavities include photonic crystal (PC), whispering gallery mode (WGM), and Fabry–Pérot (FP) cavities. Michigan Aerospace developed a WGM-based optomechanical MEMS accelerometer with a noise floor of 10 ng/$\sqrt{\text{Hz}}$ and a bandwidth of 40 Hz (Fourquette et al., 2010), as shown in Fig. 8a. National Institute of Standards and Technology (NIST) reported an FP-based optomechanical MEMS accelerometer with a noise floor of 32 ng/$\sqrt{\text{Hz}}$ and a bandwidth of 6.8 kHz (Zhou et al., 2021), as shown in Fig. 8b. Emerging optomechanical MEMS accelerometers are promising to achieve both high sensitivity and wide bandwidth.

MEMS sensors based on tunneling and electrochemical mechanisms can also be seismic-grade. Their working principles are illustrated in Fig. 9. The MEMS accelerometer (Liu and Kenny, 2001) developed by Stanford University is based on electronic tunneling effect displacement sensing and static power feedback. It is manufactured by bulk silicon fabrication technology. The working principle is shown in Fig. 9a. The noise level of the MEMS accelerometer is 20 ng/$\sqrt{\text{Hz}}$, and the frequency response range is 5–1500 Hz. The main difference between electrochemical MEMS seismic sensors and the above-mentioned MEMS accelerometers is that the former sensors take a liquid electrolyte as the inertial mass. The electrolyte is usually sealed by two pieces of rubber film in a tube with porous electrodes in the middle. When the electrolyte is subjected to external vibration, convection is formed near the electrode, resulting in the change of ion concentration and thus the current output, as shown in Fig. 9b. The electrochemical MEMS seismometer developed by the Institute of Electronics, Chinese Academy of Sciences (Deng et al., 2015) has a noise level of 3.2 ng/$\sqrt{\text{Hz}}$@0.02 Hz and a frequency response range of 0.01 Hz–20 Hz.
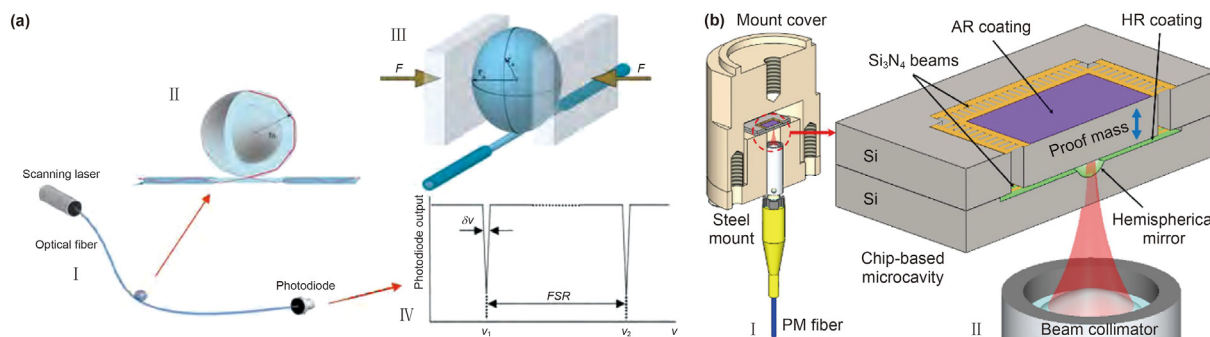
Fig. 8. Optomechanical MEMS accelerometers. (a) Michigan Aerospace (Fourquette et al., 2010); (b) NIST (Zhou et al., 2021).
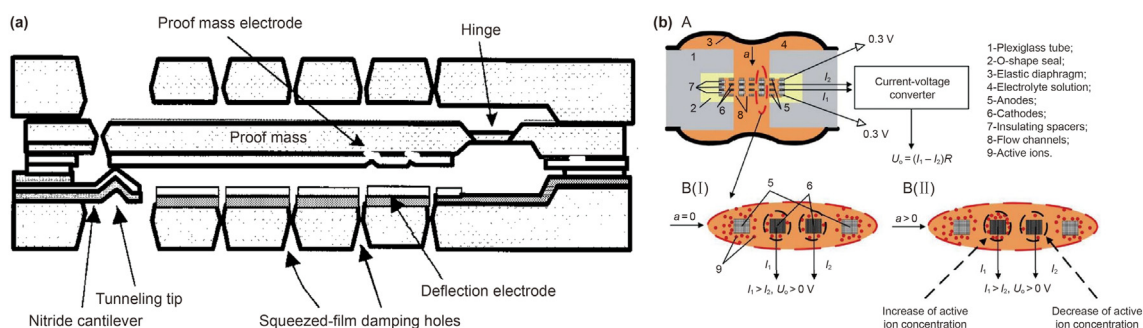

Fig. 9. Other principle-based seismic-grade MEMS accelerometers. (a) Tunneling accelerometer by Stanford (Liu and Kenny, 2001). (b) Electrochemical seismometer by IoE, CAS (Deng et al., 2015).

Other optical seismic-grade accelerometers and emerging resonant accelerometers, capable of gravity measurement, are described in the next section about MEMS gravimeters.

This section updates the state-of-the-art MEMS accelerometers for seismology, however, more specified reviews for high-performance MEMS accelerometers can be found in the author's previous article (Wang et al., 2020) and other review articles (Hou et al., 2021; D'Alessandro et al., 2019).

3.1.3. MEMS gravimeters

In 2016, a group from University of Glasgow reported a prototype of a miniaturized relative gravimeter based on MEMS technology (Middlemiss et al., 2016), which attracted considerable interest in developing MEMS high-performance accelerometers for gravity measurement. The first prototype is shown in Fig. 10. The core sensitive unit is a non-linear silicon-based flexible geometric structure forming a vibration isolation system similar to that used in gravitational wave detectors, which is fabricated by deep reactive silicon etching (DRIE) process. It has an intrinsic resonant frequency as low as 2.3 Hz under 1 g gravity. Using a highly stable optical displacement sensor, the MEMS relative gravimeter prototype achieved a sensitivity of 40 μGal/$\sqrt{Hz}$@1 Hz and a drift of 150 μGal/day (1 Gal = 1 cm/s^2 ~ 1 mg). The correlation coefficient between the measured Earth tidal signal for eight days and the theoretical tides model was 0.86. The prototype is based on an optical shadow displacement transducer whose noise floor is 2 nm/$\sqrt{Hz}$@1Hz. In order to meet the requirements of the "NEWTON-g" project, a new version with a capacitive displacement transducer is under development (Carbone et al., 2020).

In 2018, researchers from Imperial College London (Pike et al., 2018) claimed the developed MEMS seismometer for NASA's InSight Mars lander clearly monitored the Earth tides, as shown in Fig. 11. The reported MEMS seismometer has a noise floor of 0.25 μGal/$\sqrt{Hz}$ from 0.1 to 10 Hz. If an mK-level temperature control system is applied, this sensor can be used for gravity measurements.

In 2019, a group from HUST reported a more practical MEMS gravimeter that has a higher sensitivity of 8 μGal/$\sqrt{Hz}$ and a larger dynamic range of 8000 mGal using a quasi-zero stiffness suspension design and a customized optical displacement transducer. The reported MEMS gravimeter performed the co-site Earth tides measurement with a commercial superconducting gravimeter GWR iGrav for six days with the results showing a correlation coefficient of 0.91 (Tang et al., 2019). The same research group reported another MEMS gravimeter based on capacitive displacement sensing in 2021. The reported MEMS gravity sensor exhibits an ultra-low self-noise floor of 1 μGal/$\sqrt{Hz}$@1Hz, as well as excellent stability, with an Allan deviation of 3 μGal (40 s integration time). The sensor is capable of measuring the Earth tides in a 16-day span (Xu et al., 2021). Their photos are shown in Fig. 12.

In 2020, University of Cambridge developed a differential vibrating beam MEMS accelerometer demonstrating excellent long-term stability for applications in gravimetry. The MEMS gravimeter, as shown in Fig. 13, demonstrates an output Allan deviation of 9 μGal for a 1000 s integration time, a noise floor of 100 μGal/$\sqrt{Hz}$, and measurement over the full 1 g dynamic range. The correlation coefficient between the measured Earth tidal signal for four days and the theoretical tides model was 0.92 (Mustafazade et al., 2020). In 2021, the same group reported an updated version with a noise floor of 10 ng/$\sqrt{Hz}$ and a bandwidth of 50 Hz (Pandit et al., 2021), which is illustrated in Fig. 13. In addition, a spin-off company from this group called Silicon Microgravity Ltd (https://silicong.com/), was established to commercialize the MEMS resonant gravimeter.

In 2021, a research group from Tsinghua University developed a resonant MEMS accelerometer for gravity measurement, as shown in Fig. 14. The experimental results show that the MEMS
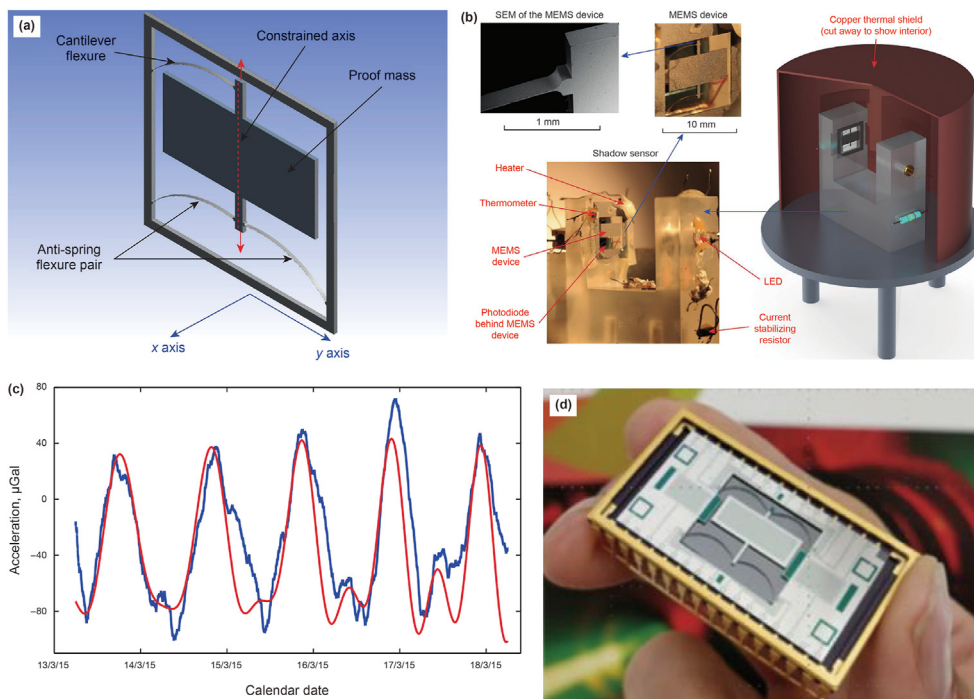
Fig. 10. MEMS relative gravimeters developed by University of Glasgow (Middlemiss et al., 2016; Carbone et al., 2020). (a) Anti-spring gravity sensing element; (b) The original experimental set-up; (c) Earth tides measurement; (d) Newly developed capacitive version.
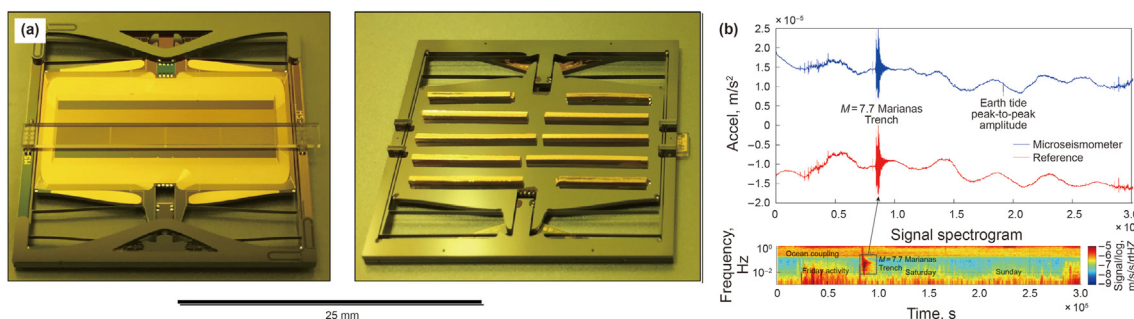

Fig. 11. MEMS relative gravimeters developed by Imperial College London (Pike et al., 2018). (a) Photographs of the MEMS chip; (b) measured seismic and tides signal.
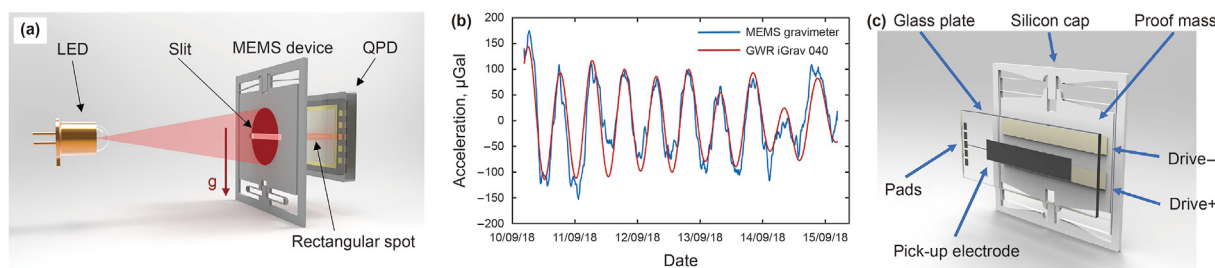

Fig. 12. MEMS relative gravimeters developed by HUST (Tang et al., 2019; Xu et al., 2021). (a) The experimental set-up; (b) The Earth tides measurement; (c) The capacitive version.

accelerometer has a noise floor down to 75 μGal/$\sqrt{\text{Hz}}$ by setting a relatively low range of ±5 g (~5000 Gal). The experimental results of the resonant accelerometer show that the averaged bias stability for one day duration is 197 μGal and the bias repeatability within about three months is 1.56 mGal. The correlation coefficient between the measured Earth tidal signal for six days and the theoretical tides model was 0.84 (Fang et al., 2021).

Currently, MEMS relative gravimeters based on capacitive, optical, and resonant principles have all successfully demonstrated the ability to measure Earth tides. Their sensitivities (noise floors) vary from 0.25 μGal/$\sqrt{\text{Hz}}$ to 100 μGal/$\sqrt{\text{Hz}}$ and their short-term stability is in the range of 10 μGal to 200 μGal, as shown in Table 2. Although their performance is not as good as the conventional relative gravimeters such as CG-6 and gPhone X from Micro-
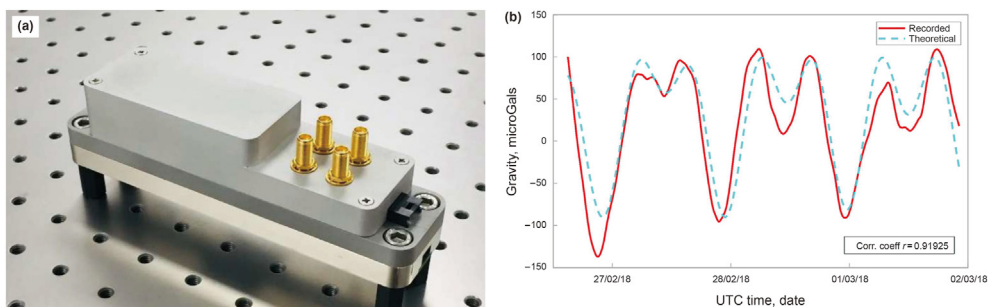
Fig. 13. MEMS relative gravimeters developed by University of Cambridge (Mustafazade et al., 2020). (a) Packaged MEMS sensing element; (b) measured Earth tides signal.
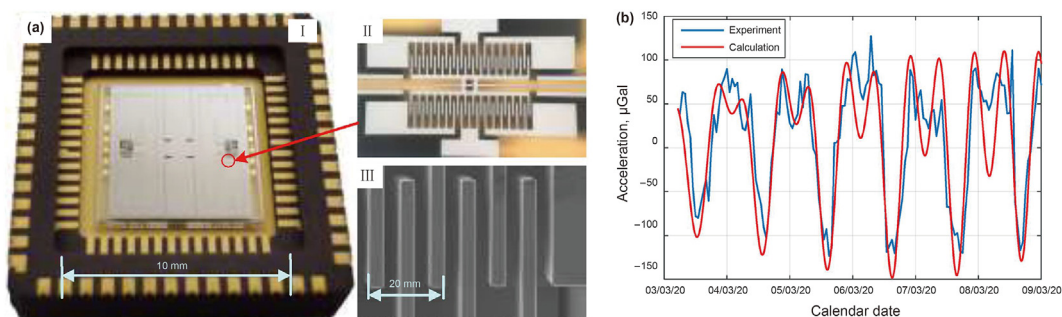

Fig. 14. MEMS relative gravimeters developed by Tsinghua University (Fang et al., 2021). (a) Packaged MEMS sensing element; (b) measured Earth tides signal.

g LaCoste, the emerging MEMS gravimetry technology are promising to be a good solution for low-cost and precise gravity measurement for geophysical and exploration applications.

3.2. MEMS tiltmeters

MEMS tilt sensors or inclinometers are based on high-resolution MEMS accelerometers by measuring the Cartesian component of gravitational acceleration. However, due to the inherent angle-to-gravity trigonometric relationship, the linear measurement range of the tilt sensor based uniaxial accelerometer can only be ±20°~±30° (Luczak et al., 2006). State-of-the-art commercial MEMS tiltmeters include SCA103T (Murata-SCA103T-D04) from Murata with a resolution of 0.0013° in a 10-Hz bandwidth and a linear measurement range of ±30°, Jewell DMH (Jewell-DMH) with a resolution of 0.001° and a measurement range of ±60°, and ADXL 203 (Analog Devices-ADXL203) from Analog Devices with a resolution of 0.06° in a 60-Hz bandwidth; the latter has been applied on the seismic experiments on the InSight Mars lander for tilt measurement on Mars (Lognonné et al., 2019). The MEMS capacitive tiltmeter (Rao et al., 2020), as shown in Fig. 15, is based on area-variation capacitive sensing, and has a linear measurement range of ±30° with a non-linearity of ±2.8%, a bandwidth of 100 Hz and an angle resolution of 0.0007° with 0.5 s integral time, which is better

than commercial MEMS tiltmeters. The state-of-the-art angle resolution of MEMS tiltmeters is $2.86 \times 10^{-5\circ}$, which is achieved by a MEMS resonant accelerometer (MRA) (Zou et al., 2014). The resonant frequency of MRAs is shifted due to an axial stress generated by the proof mass under an applied tilt angle. MRAs possess many advantages of quasi-digital output, high sensitivity, and a large dynamic range. However, MRA chips have to be vacuum packaged and require complex circuits for frequency stabilization and automatic gain control.

In order to increase the linear measurement range, an effective way is to apply more gravitational-acceleration-sensing elements in perpendicular or radial arrangement either with a single movable mass (Wang et al., 2018; Ding et al., 2019) or separate masses (Li et al., 2016). The entire 0°–360° tilt measurement can be fully covered by applying inverse trigonometric calculation and angle segmental combination on the outputs of each sensing element, as shown in Fig. 16. The reported MRA MEMS full angle range tilt-meter has an angle resolution of 0.002° with 5 s integral time (Wang et al., 2018).

In addition, an ultra-sensitive and stable MEMS tiltmeter was reported, as shown in Fig. 17, which is based on a 0.7 Hz quasi-zero-stiffness suspension system with capacitive displacement sensing, having an angle resolution of $2.29 \times 10^{-8\circ}$ with 30 s integral time (Wu et al., 2020). The measured tidal tilt signal of eleven days

Table 2
Comparison of the developed MEMS relative gravimeters.

| Device	Spring	Sensing	Bandwidth	Sensitivity	Ref.
Glasgow-2016	Nonlinear	Optical	2.3 Hz	40 μGal/√Hz	Middlemiss et al. (2016)
Glasgow-2020	Nonlinear	Capacitive	7.3 Hz	6 μGal/√Hz	Carbone et al. (2020)
Imperial-2018	Linear	Capacitive	40 Hz	0.25 μGal/√Hz	Pike et al. (2018)
HUST-2019	Nonlinear	Optical	3.1 Hz	8 μGal/√Hz	Tang et al. (2019)
HUST-2021	Linear	Capacitive	14.5 Hz	1 μGal/√Hz	Xu et al. (2021)
Cambridge-2020	Linear	Resonant	50 Hz	100 μGal/√Hz	Mustafazade et al. (2020)
Tsinghua-2021	Linear	Resonant	50 Hz	75 μGal/√Hz	Fang et al. (2021)
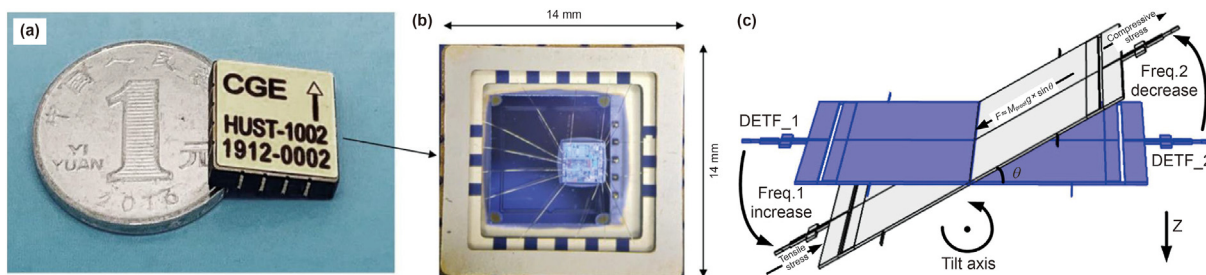
Fig. 15. MEMS tilt sensors by different research groups: (a) Capacitive tiltmeter by HUST (Rao et al., 2020); (b) resonant tiltmeter by Cambridge (Zou et al., 2014).
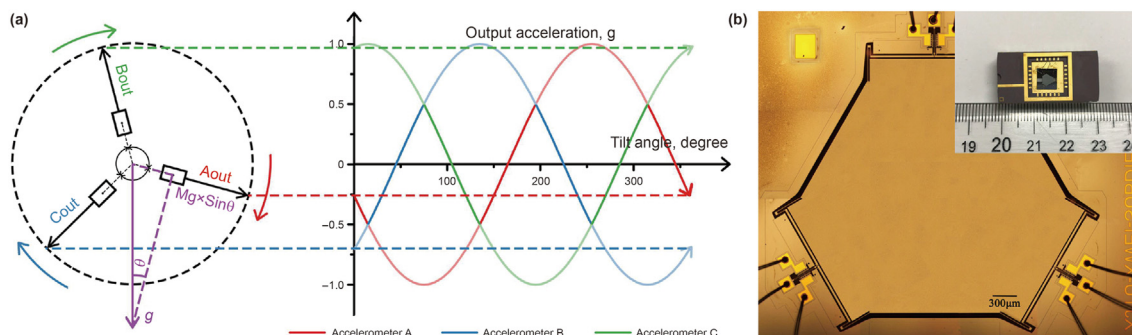

Fig. 16. MEMS tiltmeter developed by XJTU (Wang et al., 2018). (a) Working principle of a 360° measurement; (b) MEMS tilt sensor chip.
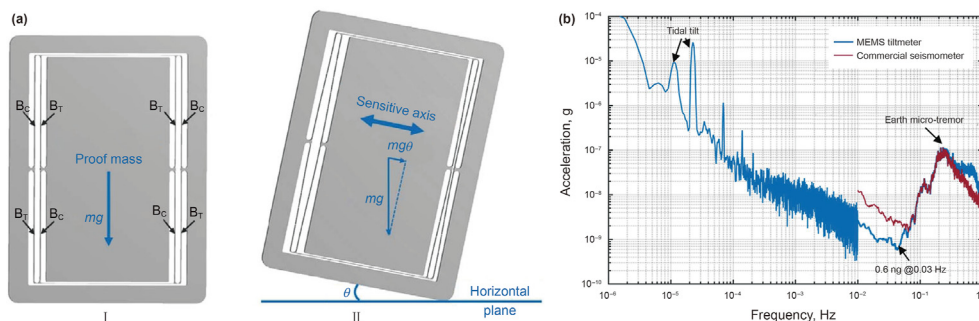

Fig. 17. MEMS Earth tidal tiltmeter developed by HUST (Wu et al., 2020). (a) MEMS sensing element; (b) measured Earth tidal tilt.

demonstrates a correlation coefficient of 0.87 with the Earth tidal tilt theoretical model. Since this sensor has a very limited measurement range of 0.004°, it is developed for specialized applications, such as volcano activity monitoring and reservoir dam deformation monitoring.

As shown in Table 3, commercial MEMS tiltmeters with a resolution of 0.001° are comparable with Jewell's DXI series, and the MRA tiltmeter can reach a comparable performance of Jewell's LCF series with a resolution of $5.7 \times 10^{-5\circ}$ (Jewell-LCF). MEMS

tiltmeters have comparable performance with the tiltmeters developed by conventional technologies; therefore, they are promising to be widely used in geophysical and resource exploration fields.

3.3. MEMS magnetometers

MEMS magnetometers for exploration and geophysical applications can be classified as micro fluxgate sensors, Hall sensors,

Table 3
Comparison of the MEMS tiltmeters with conventional tiltmeters.

Device	Technology	Resolution	Linear range	Ref.
Murata SCA103T	MEMS	0.0013°	±30°	(Murata-SCA103T-D04)
Jewell DMH	MEMS	0.001°	±60°	(Jewell-DMH)
ADI ADXL203	MEMS	0.06°	±30°	(Analog Devices-ADXL203)
HUST	MEMS	0.0007°	±30°	Rao et al. (2020)
Cambridge	MEMS	$2.86 \times 10^{-5\circ}$	±30°	Zou et al. (2014)
XJTU	MEMS	0.02°	±180°	Wang et al. (2018)
HUST	MEMS	$2.29 \times 10^{-8\circ}$	±0.004°	Wu et al. (2020)
Jewell DXI-100	For.-Bal.	0.001°	±60°	(Jewell-DXI)
Jewell LCF-2000	For.-Bal.	$5.70 \times 10^{-5\circ}$	±90°	(Jewell-LCF)

magneto-resistance sensors, and resonant magnetometers. The challenges of micro fluxgate sensors include the miniaturization of solenoid coils and the integration of magnetic cores. Gu et al. (2019) reported a MEMS fluxgate sensor with alloy solenoid coils by MEMS casting technology, reducing the chip size and the fabrication cost. Lei et al. (2018) reported a MEMS fluxgate sensor with a co-based amorphous core having a noise floor of 110 pT/$\sqrt{\text{Hz}}$@1Hz. Although the noise floor of MEMS fluxgate sensors (shown in Fig. 18) is higher than that of conventional fluxgate sensors (typically 100 fT/$\sqrt{\text{Hz}}$ ~10 pT/$\sqrt{\text{Hz}}$), they are promising to be widely used due to their small-size and low-cost.

Hall-effect-based magnetic sensors became widely used due to their compatibility with low-cost complementary metal-oxide-semiconductor (CMOS) semiconductor technologies. Min et al. (2011) reported a 0.6 mm^2 monolithic hall sensor with both the hall plate and the readout circuit fabricated by a 0.18 μm CMOS process, resulting in a noise floor of 25 μT/$\sqrt{\text{Hz}}$. Although hall sensors are less sensitive compared with other MEMS magnetometers, the silicon-based fabrication process can offer an extended operating temperature range to more than 600 K (Leonov et al., 2016); therefore, they can be used in borehole measurement of the oil and gas exploration.

Magneto-resistance sensors use the fact that the electrical resistance in a ferromagnetic thin-film alloy is changed through an external magnetic field (Yang and Zhang, 2021), as shown in Fig. 19. They can be categorized as anisotropic magneto-resistance (AMR), giant magneto-resistance (GMR), and tunneling magneto-resistance (TMR) sensors, which are generally manufactured by magnetic materials thin-film deposition technologies. AMR sensors are typically used for measuring weak magnetic fields with the strength from 2 nT to 1 mT (Novotný et al., 2018). AMR sensors have reasonably high sensitivity and are much less expensive than conventional fluxgate sensors; however, AMR sensors generally get saturated under mT-level magnetic field so they require complex Set/Reset procedures. GMR sensors are sensitive to a magnetic field between 1 nT and 100 mT and can work under a high temperature of about 500 K. However, GMR sensors can be permanently destroyed by a large magnetic field of 1 T or above (Ripka, 2008). TMR sensors have better performance than Hall, AMR, and GMR sensors in terms of sensitivity, temperature coefficient, power consumption, and linearity. The sensitivity of TMR sensors can be 5-times of GMR sensors and 20-times of AMR sensors. For example, the TMR9112 sensor available from the Chinese company MDT Ltd.

has a noise floor of 150 pT/$\sqrt{\text{Hz}}$@1Hz and a saturation field of ±0.8 mT (MDT-TMR9112).

Another emerging MEMS magnetometer senses the frequency shifts of micro-resonators encountering the Lorentz force under a magnetic field; this is illustrated in Fig. 20. Unlike magneto-resistance and Hall-effect sensors, MEMS resonant Lorentz-force magnetometers are advantageous in terms of sensitivity, high resolution, compatibility with standard MEMS fabrication processes, and immunity to magnetic hysteresis. Researchers from HUST (Wang et al., 2021) reported a noise floor of 210 nT/$\sqrt{\text{Hz}}$@1Hz, under a background magnetic field of 0.13 T.

Unlike MEMS accelerometers and tiltmeters, MEMS magnetometers are further way from being applied to geophysical and resource exploration fields. Low noise is still a major challenge for MEMS magnetometers, as can be seen from a comparison shown in Table 4.

3.4. MEMS angular accelerometers

An angular accelerometer is a kind of inertial sensor sensitive to rotational acceleration. Angular acceleration measurement for geophysical applications requires a low noise level of 1 rad/s^2/$\sqrt{\text{Hz}}$ or even below. As mentioned before, gyroscopes can also be used for rotation measurement; however, gyroscopes require a time-differentiation operation to obtain angular accelerations. In addition, the performance of MEMS gyroscopes is still far behind macroscopic fiber and laser gyroscopes, and usually cannot meet the requirements of geophysical applications.

Currently, commercial MEMS angular accelerometers are only available from ST Microelectronics and Dephi Technologies. ST's LIS1R02 is a capacitive angular accelerometer with a resolution of 2.5 rad/s^2, a bandwidth of 30−800 Hz, and a maximum acceleration measurement of 200 rad/s^2 (Gola et al., 2001). Dephi's RV200L is a spring torque-balanced angular accelerometer that is also based on capacitive displacement sensing, having a resolution of 5 rad/s^2, a bandwidth of 10−800 Hz, and a maximum acceleration measurement of 400 rad/s^2 (US Patent US6666092B2). Both can be used for control of hard-drive disk (HDD) head positions and for the detection of automotive accidents.

Research work on MEMS angular accelerometers has been conducted by several universities and companies. Similar to most MEMS translational accelerometers, some MEMS angular accelerometers are also based on spring-mass systems but employ a rotary
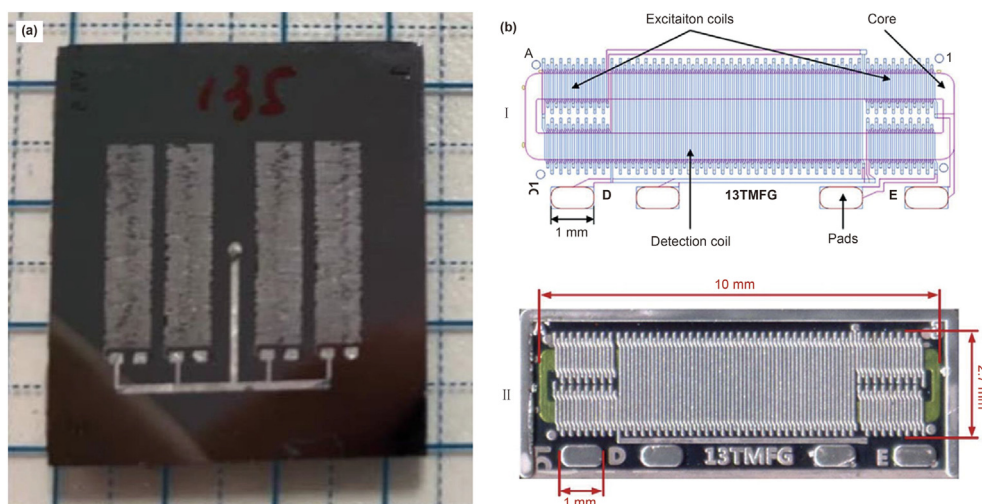

Fig. 18. MEMS fluxgate magnetometers. (a) Micro-fluxgate sensor by SIMIT (Gu et al., 2019); (b) micro-fluxgate sensor by SJTU (Lei et al., 2018).
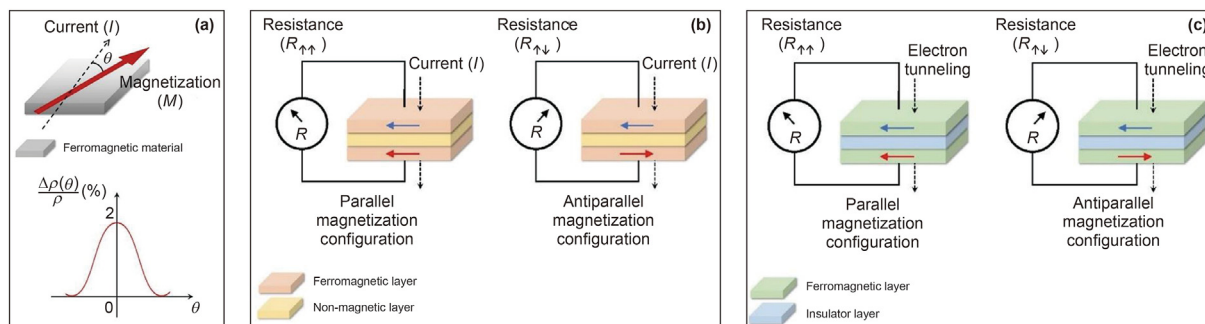
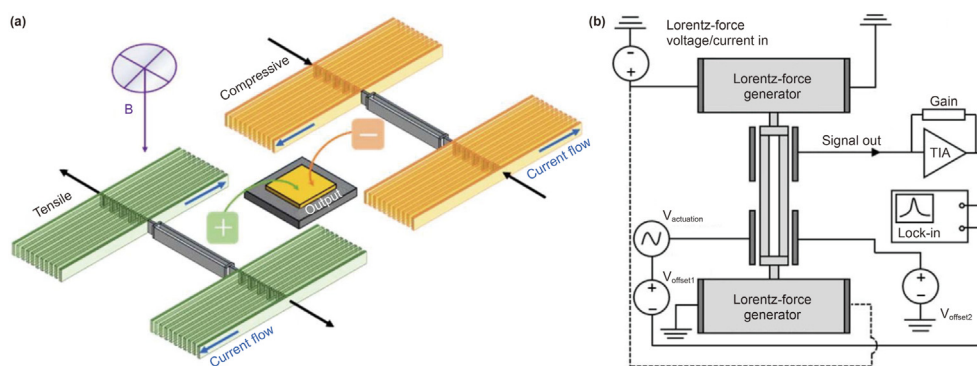**Fig. 19.** Working principles of magnetoresistance sensors (Yang and Zhang, 2021). (a) AMR; (b) GMR; (c) TMR.

Fig. 20. Working principles of MEMS resonant Lorentz-force magnetometers (Wang et al., 2021).

Table 4
Comparison of the high-performance MEMS magnetometers.

Device	Technology	Noise @1 Hz	Range	Ref.
SJTU	Fluxgate	110 pT/$\sqrt{Hz}$	±95 µT	Lei et al. (2018)
Korea Uni.	Hall	25 µT/$\sqrt{Hz}$	±400 mT	Min et al. (2011)
Czech Tech. Uni.	AMR	150 pT/$\sqrt{Hz}$	±150 µT	Novotný et al. (2018)
AAL002	GMR	10 nT/$\sqrt{Hz}$	±150 µT	Michelena (2013)
MDT TMR9112	TMR	150 pT/$\sqrt{Hz}$	±800 µT	(MDT-TMR9112)
HUST	Resonant	210 nT/$\sqrt{Hz}$	±130 mT	Wang et al. (2021)

disk and a pendulum approach. Researchers from University of Michigan (O'Brien et al., 2003) developed a dual-anchor supported rotary disk angular accelerometer, whose displacement is sensed by a capacitive transducer. This sensor has a resolution of 1 rad/s^2, a bandwidth of 250 Hz, and a maximum acceleration measurement of 350 rad/s^2. The oilfield service company Schlumberger also developed a MEMS angular accelerometer based on the rotary disk approach. The sensor is used for correcting errors and perturbations of drilling tools under ambient vibrations and has a high resolution of 3 mrad/s^2 and a bandwidth of 60 Hz−250 Hz (Projetti et al., 2014). Based on torsion-balanced pendulums, researchers from University of California, Irvine (Eklund and Shkel, 2005) developed a piezoresistive angular accelerometer while researchers from Beijing University of Aeronautics and Astronautics (BUAA) (Li et al., 2013) developed a capacitive counterpart. The structures of these four angular accelerometers are shown in Fig. 21. The MEMS angular accelerometer developed by Liu and Pike (2016) from Imperial College London, as shown in Fig. 22, uses an in-plane see-saw sensitive structure, which is fabricated by a DRIE process and has differential area-variation capacitive displacement sensing. It has a resolution of better than 0.003 rad/s^2, a bandwidth of 0.1−10 Hz and a measurement range of 200 rad/s^2. Furthermore,

there are also some liquid-mass based bionic MEMS angular accelerometers reported. Similar to the vestibular systems of animals, the fluid in a semicircular or circular channel lags behind the channel when there is a rotational vibration due to inertia. The relative motion between the fluid and the channels can be sensed by either a pressure sensor at the end of the channel (US Patent US 20030047002A1US Patent US 20030047002A1), a thermal transducer (Groenesteijn et al., 2014), or piezoresistive cantilevers (Takahashi et al., 2019).

Compared with the conventional force-balanced angular accelerometer, such as the most accuracy ASMP series of its class in the world claimed by Jewell (Jewell-ASMP), the high-performance MEMS angular accelerometers have comparable performance, as listed in Table 5. Therefore, MEMS angular accelerometers show promise to be used for oil well drilling and other geophysical applications.

3.5. MEMS gravity gradiometers

Currently, there are only several monolithic MEMS-based gravity gradiometer prototypes reported, which are based on either a differential-accelerometer approach or a torsion-balance method with a working principle (Liu et al., 2016) shown in Fig. 23.

In 2009, Flokstra et al. (2009) from University of Twente developed a MEMS gravity gradiometer based on the differential-accelerometer approach. Two identical accelerometers were fabricated as a monolithic chip (80 mm × 80 mm) on a 4-inch silicon wafer. Each accelerometer has a proof mass of 20 g, achieved by attaching gold blocks on silicon. The masses are suspended by four spring beams and the displacement is sensed by gap-variation comb capacitive transducers. The structure is shown in Fig. 24. The resonant frequency of each accelerometer is above 1 Hz and can sustain Earth gravity. With a low temperature of 77 K and a
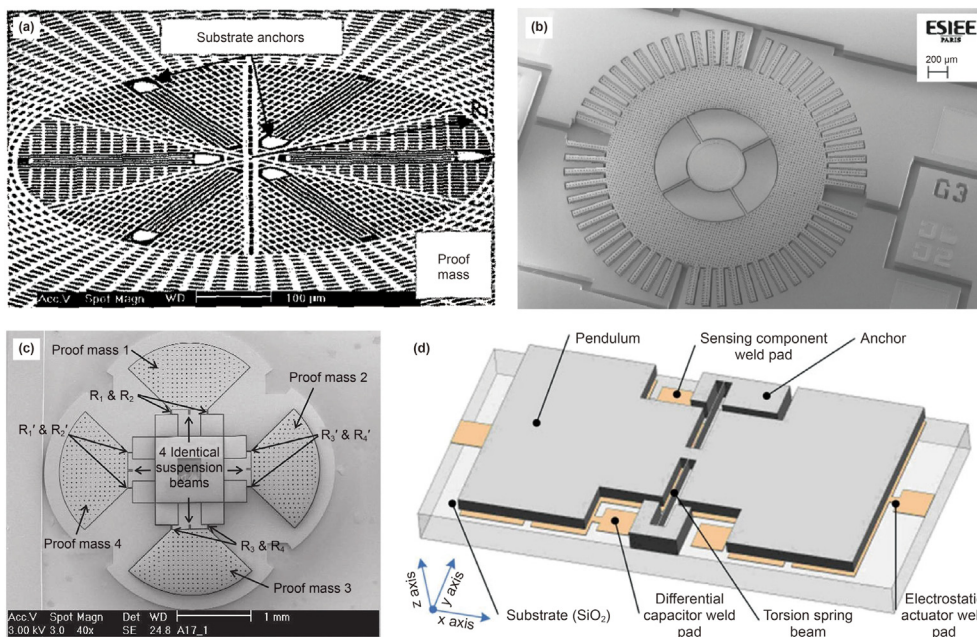
Fig. 21. MEMS angular accelerometers. (a) University of Michigan, rotary disk (O'Brien et al., 2003); (b) Schlumberger, rotary disk (Projetti et al., 2014); (c) UC Irvine, pendulum (Eklund Shkel, 2005); (d) BUAA, pendulum (Li et al., 2013).
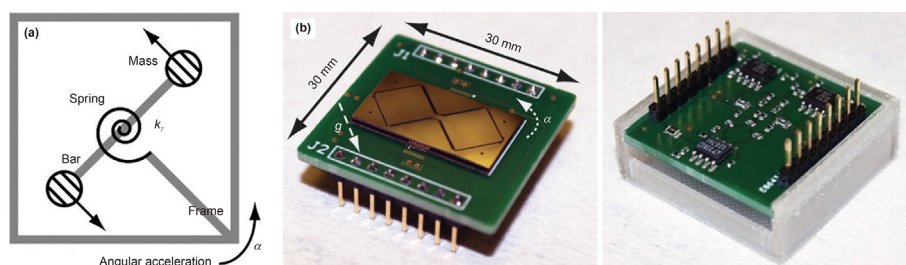

Fig. 22. MEMS angular accelerometer developed by Imperial College London (Liu and Pike, 2016).

Table 5
Comparison of MEMS angular accelerometers with conventional accelerometers.

Device	Technology	Bandwidth	Resolution	Range	Ref.
ST LIS1R02	MEMS	30 Hz—800 Hz	2.5 rad/s^2	200 rad/^{2}	(STMicroelectronics-L6671)
Dephi RV200L	MEMS	10 Hz—800 Hz	5 rad/s^2	400 rad/^{2}	(US Patent US6666092B2)
Michigan	MEMS	DC ~800 Hz	1 rad/s^2	350 rad/^{2}	O'Brien et al. (2003)
Schlumberger	MEMS	60 Hz—250 Hz	0.003 rad/s^2	–	Projetti et al. (2014)
Imperial College	MEMS	0.1 Hz—10 Hz	0.003 rad/s^2	200 rad/^{2}	Liu and Pike (2016)
Jewell ASMP	Force-Bal.	DC ~70 Hz	0.004 rad/s^2	200 rad/^{2}	(Jewell-ASMP)

high-quality factor of 1×10^5, this sensor can have a thermal noise floor of 107 mEö/$\sqrt{\text{Hz}}$, and a total noise floor of 119 mEö/$\sqrt{\text{Hz}}$ in theory (1 Eö = 10^{-9}/s^2).

In 2009, another monolithic MEMS gravity gradiometer, which is based on the pendulum torsion-balance approach, was developed by EPFL (Ghose and Shea, 2009). The first prototype has a short spring beam bridging the pivot anchor and the proof-mass pendulum and is sensitive to in-plane rotations with a fundamental frequency of 1.35 Hz. However, the first prototype exhibited considerable out-of-plane sag displacement of 15 μm under Earth's gravity, resulting in misalignment and spurious vibration issues. In order to overcome these issues, a second prototype was designed to minimize the out-of-plane sag to 2.5 μm under Earth's gravitational

acceleration. The second prototype (Ghose, 2012) reported in 2012 has a mass pendulum suspended by two spring beams and is sensitive to out-of-plane rotations with a fundamental frequency of 1.5 Hz. The structures of both prototypes are shown in Fig. 25. The displacement of both prototypes along their compliant directions is sensed by gap-variation capacitive transducers. However, the noise of the equivalent gravity gradient of both prototypes was not reported.

All above-mentioned MEMS gravity gradiometers are designed for space applications. Twente's device is for global gravity mapping, while EPFL's devices are Earth sensors for determining the attitude of satellites. However, none of them can be operated on Earth. In order to conduct ground validation before space
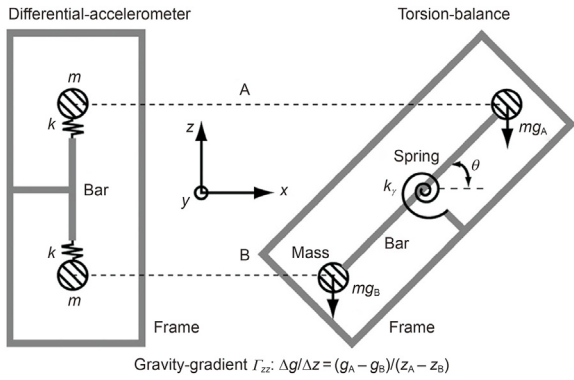
Gravity-gradient Γ_{zz}: $\Delta g/\Delta z = (g_A - g_B)/(z_A - z_B)$

Fig. 23. Working principle of monolithic MEMS gravity gradiometers (Liu et al., 2016).

deployment and gravity exploration on Earth, the gradiometer has to bear Earth gravity. To solve this issue, a MEMS gravity gradiometer capable of operation over a range of gravity from 0 g to 1 g was developed by Imperial College London (Liu et al., 2014, 2016). As shown in Fig. 26, a seesaw-lever force-balancing suspension is designed with a low fundamental frequency for in-plane rotation to respond to a gravity gradient. During operation under 1 g, a gravitational force is axially loaded on two straight beams that perform as a stiff fulcrum for the mass-connection lever without affecting sensitive in-plane rotational sensing. The proposed MEMS gravity gradiometer has a fundamental frequency of 6.6 Hz, and the theoretical noise floor of 10 Eö/$\sqrt{\text{Hz}}$ on conditions of achieving a high-quality factor of 10^5 at room temperature and vacuum (Liu et al., 2016).

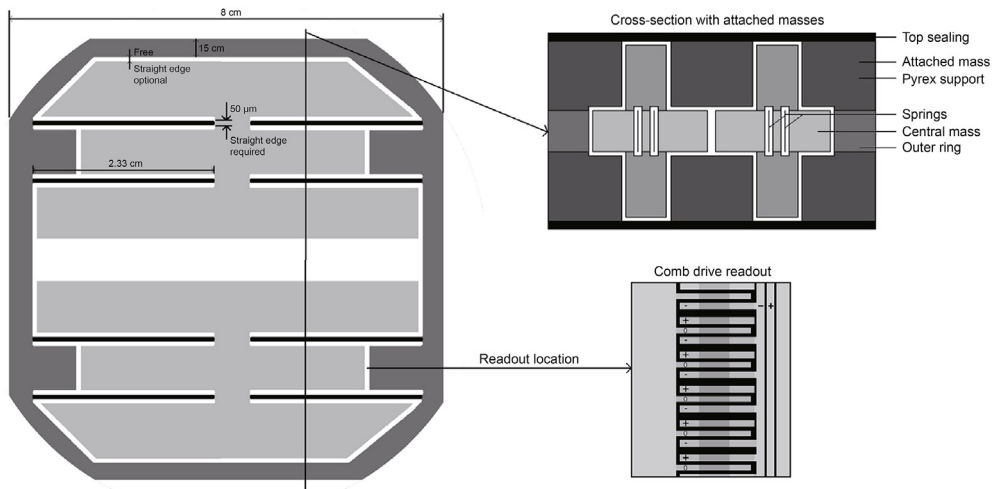Two other torsion-balance-based MEMS gravity gradiometer

Fig. 24. A monolithic MEMS gravity gradiometer from University of Twente based on the differential-accelerometer approach with a gold block of 20 g on each accelerometer (Flokstra et al., 2009).
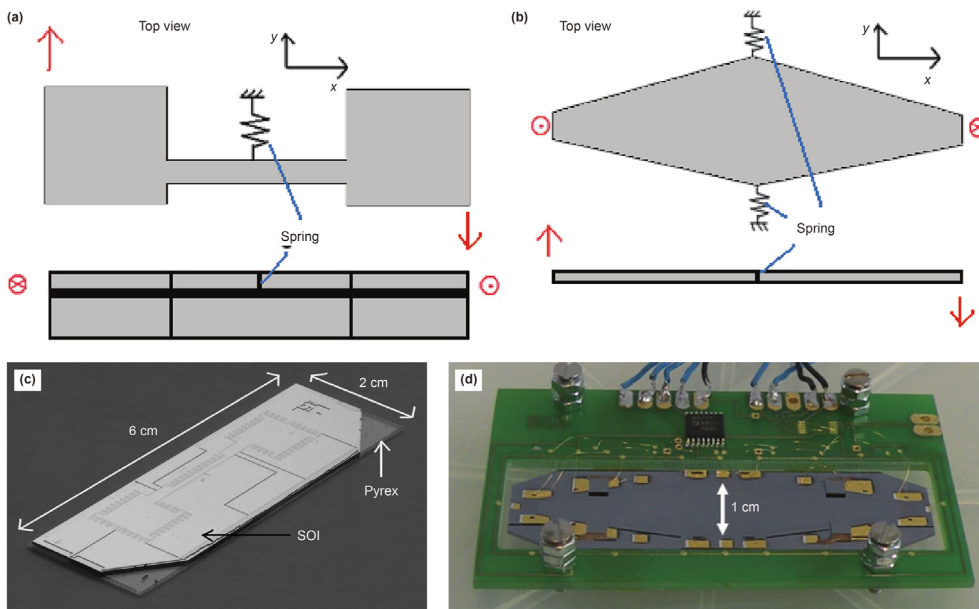

Fig. 25. Prototypes of EPFL's monolith MEMS gravity gradiometers based on the pendulum torsion-balance approach (Ghose, 2012). (a) The 1st prototype schematic; (b) the 2nd prototype schematic; (c) fabricated 1st prototype; (d) fabricated 2nd prototype.
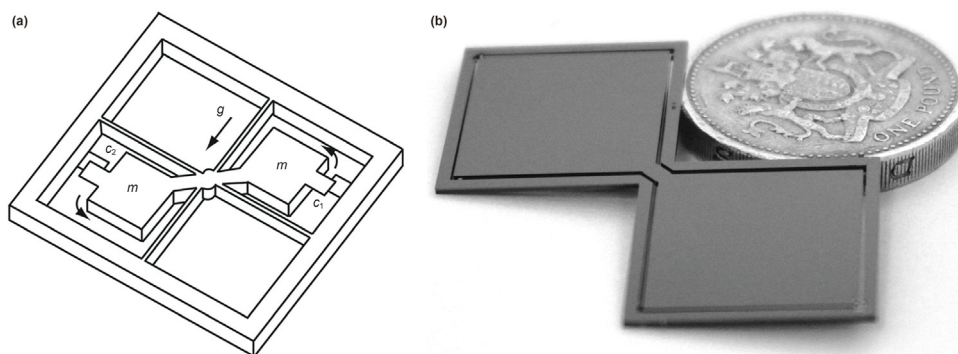
Fig. 26. MEMS gravity gradiometer developed by Imperial College London (Liu et al., 2016). (a) Working principle of the gravity gradient sensor; (b) fabricated MEMS gravity gradient sensor chip.
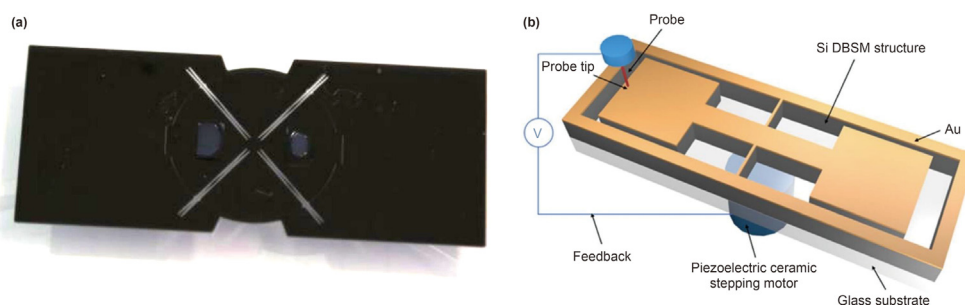

Fig. 27. Other MEMS gravity gradiometers for satellite attitude measurement from (a) University of Glasgow (Marocco et al., 2019), and (b) Tsinghua University (Cao et al., 2021).

prototypes were designed for satellite attitude determination. Marocco et al. (2019) from University of Glasgow reported a MEMS gravity gradiometer with capacitive displacement sensing and Cao et al. (2021) from Tsinghua University reported a MEMS gravity gradiometer with tunneling displacement sensing. Both structures are shown in Fig. 27.

Based on all the observations, it can be summarized that MEMS gravity gradiometers are still in the prototyping stage. Compared to other reported MEMS sensors, they are further away from practical applications in geophysical and resource exploration fields.

4. Conclusions

This review article comprehensively analyzes the sensor requirements for geophysical and resource exploration, including earthquake monitoring, seismic exploration, gravity exploration, magnetic exploration, drilling process monitoring, Earth tides, volcanic activity monitoring, and gravity-aided navigation. Basics of MEMS technology are also introduced with a brief history of the MEMS technology development and applications. Then, the research status of related MEMS sensors is described in detail, both for commercial products as well as for research prototypes. The following conclusion can be drawn: MEMS seismometers have been employed to monitor weak earthquakes, and even Marsquakes by the InSight's short-period seismometer. MEMS seismic-grade accelerometers developed by Sercel, have been used for on-shore and off-shore seismic exploration. MEMS gravimeters have successfully demonstrated Earth tides measurement. Several ambitious projects, such as the "NEWTON-g" project, plan to develop a hybrid gravity measurement system that has an array of low-cost MEMS relative gravimeters anchored on an absolute quantum gravimeter for real-time monitoring the evolution of the subsurface mass changes. MEMS tiltmeters and angular

accelerometers have demonstrated comparable performance with conventional force-balanced sensors produced by the leading company Jewell Instruments and are promising to be widely used for cost-sensitive applications. MEMS magnetometers still have the issue of a higher noise floor, which is one or two orders higher than conventional fluxgate sensors used for geophysical applications. Therefore, MEMS magnetometers still require more effort on development. MEMS gravity gradiometers are in the prototyping stage with the main challenge of achieving a higher resolution and most reported work targeted for space applications such as satellite attitude determination. Hence, MEMS gravity gradiometers are further away from being applied in geophysical and resource exploration fields. Overall, there are several off-the-shelf or fully developed high-performance MEMS sensors that can be used in the above-mentioned geophysical and exploration applications. Especially for applications requiring low cost for large-scale deployment, MEMS sensors have a bright future.

References

Abdolvand, R., Amini, B.V., Ayazi, F., 2007. Sub-micro-gravity in-plane accelerometers with reduced capacitive gaps and extra seismic mass. J. Microelectromech. Syst. 16 (5), 1036–1043. https://doi.org/10.1109/JMEMS.2007.900879.

Affleck, C.A., Jircitano, A., 1990. Passive gravity gradiometer navigation system. In: IEEE symposium on position location and navigation. A Decade of Excellence in the Navigation Sciences, pp. 60–66. https://doi.org/10.1109/PLANS.1990.66158.

Analog Devices. ADXL 203. datasheet. URL. https://www.analog.com/en/products/adxl203.html#product-overview.

Beeby, S., Ensel, G., White, N.M., et al., 2004. MEMS Mechanical Sensors. Artech House, Boston.

Boom BA, Bertolini A, Hennes E, et al. Nano-G accelerometer using geometric anti-springs. 2017 IEEE 30th International Conference on Micro Electro Mechanical Systems (MEMS). vol. 2017; 33-36. doi: 10.1109/MEMSYS.2017.7863332.

Cao, Y.L., Zhao, J.H., Xing, F., You, Z., 2021. Structural process and testing of tunneling attitude sensor based on gravity gradient torque measurements. J. Micromech. Microeng. 31 (12), 125013. https://doi.org/10.1088/1361-6439/ac3467.

Carbone, D., Antoni-Micollier, L., Hammond, G., et al., 2020. The Newton-g gravity imager: towards new paradigms for terrain gravimetry. Front. Earth Sci. 8, 452. https://doi.org/10.3389/feart.2020.573396.

Chae, J., Kulah, H., Najafi, K., 2005. A monolithic three-axis micro-g micromachined silicon capacitive accelerometer. J. Microelectromech. Syst. 14 (2), 235–242. https://doi.org/10.1109/JMEMS.2004.839347.

Chen, S.J., Shen, C.H., 2008. A novel two-axis CMOS accelerometer based on thermal convection. IEEE Trans. Instrum. Meas. 57 (8), 1572–1577. https://doi.org/10.1109/TIM.2008.925347.

Cochran, E.S., Vidale, J.E., Tanaka, S., 2004. Earth tides can trigger shallow thrust fault earthquakes. Science 306 (5699), 1164–1166. https://doi.org/10.1126/science.1103961.

Colibrys, SF1500. datasheet. URL. http://datasheet.elcodis.com/pdf/46/63/466325/sf1500s.a.pdf.

D'Alessandro, A., Scudero, S., Vitale, G., 2019. A review of the capacitive MEMS for seismology. Sensors 19 (14), 3093. https://doi.org/10.3390/s19143093.

Deng, T., Chen, D., Chen, J., et al., 2015. Microelectromechanical systems-based electrochemical seismic sensors with insulating spacers integrated electrodes for planetary exploration. IEEE Sensor. J. 16 (3), 650–653. https://doi.org/10.1109/JSEN.2015.2491783.

Ding, H., Ma, Y., Guan, Y., et al., 2019. Duplex mode tilt measurements based on a MEMS biaxial resonant accelerometer. Sens. Actuators, A 296, 222–234. https://doi.org/10.1016/j.sna.2019.06.024.

Dransfield, M.H., Christensen, A.N., 2013. Performance of airborne gravity gradiometers. Lead. Edge 32 (8), 908–922. https://doi.org/10.1190/tle32080908.1.

Eklund, E.J., Shkel, A.M., 2005. Single-mask SOI fabrication process for linear and angular piezoresistive accelerometers with on-chip reference resistors. IEEE Sens. 4. https://doi.org/10.1109/ICSENS.2005.1597784, 2005.

El Mansouri, B., Middelburg, L.M., Poelma, R.H., et al., 2019. High-resolution MEMS inertial sensor combining large-displacement buckling behaviour with integrated capacitive readout. Microsysy. Nanoeng. 5 (1), 1–14. https://doi.org/10.1038/s41378-019-0105-y.

Endevco, Model 7302BM4. datasheet. URL. http://www.globalv.co.kr/data/7302BM4.pdf.

Endevco, Model 86. datasheet. URL. https://www.endevco.com/datasheets/86.pdf.

Fang, Z., Yin, Y., Chen, C., et al., 2021. A sensitive micromachined resonant accelerometer for moving-base gravimetry. Sens. Actuators, A 325, 112694. https://doi.org/10.1016/j.sna.2021.112694.

Flokstra, J., Cuperus, R., Wiegerink, R.J., et al., 2009. A MEMS-based gravity gradiometer for future planetary missions. Cryogenics 49 (11), 665–668. https://doi.org/10.1016/j.cryogenics.2008.12.019.

Fourquette, D., Otugen, V., Larocque, L.M., et al., 2008. Optical MEMS-based seismometer" WhiGS". In: 2008 Monitoring Research Review: Ground-Based Nuclear Explosion Monitoring Technologies, pp. 403–407.

Furubayashi, Y., Oshima, T., Yamawaki, T., et al., 2019. 10.2 A 22ng/√Hz 17mW MEMS accelerometer with digital noise-reduction techniques. In: 2019 IEEE International Solid-State Circuits Conference-(ISSCC), pp. 182–184. https://doi.org/10.1109/ISSCC.2019.8662331.

Ghose, K., Shea, H.R., 2009. Fabrication and testing of a MEMS based earth sensor. In: TRANSDUCERS 2009-2009 International Solid-State Sensors, Actuators and Microsystems Conference, pp. 327–330. https://doi.org/10.1109/SENSOR.2009.5285496.

Ghose, K., 2012. MEMS Inertial Sensor to Measure the Gravity Gradient Torque in Orbit. PhD Thesis. EPFL. https://doi.org/10.5075/epfl-thesis-5231.

Gola, A., Bagnalasta, N., Bendiscioli, P., et al., 2001. A MEMS-based rotational accelerometer for HDD applications with 2.5 rad/sec^2 resolution and digital output. In: Proceedings of the IEEE 27th European Solid-State Circuits Conference, pp. 321–324.

Groenesteijn, J., Droogendijk, H., de Boer, M.J., et al., 2014. An angular acceleration sensor inspired by the vestibular system with a fully circular fluid-channel and thermal read-out. In: 2014 IEEE 27th International Conference on Micro Electro Mechanical Systems (MEMS), pp. 696–699.

Gu, J., Hou, X., Xia, X., et al., 2019. Solenoid fluxgate current sensor micromachined by wafer-level melt-metal casting technique. In: 2019 IEEE 32nd International Conference on Micro Electro Mechanical Systems (MEMS), pp. 252–255. https://doi.org/10.1109/JMEMS.2020.3001928.

Haris, M., Qu, H., 2010. A CMOS-MEMS piezoresistive accelerometer with large proof mass. In: 2010 IEEE 5th International Conference on Nano/Micro Engineered and Molecular Systems, pp. 309–312. https://doi.org/10.1109/NEMS.2010.5592224.

Hindrichsen, C.C., Larsen, J., Thomsen, E.V., et al., 2009. Circular piezoelectric accelerometer for high band width application. In: 2009 IEEE SENSORS, pp. 475–478. https://doi.org/10.1109/ICSENS.2009.5398277.

Hinze, W.J., Von Frese, R.R.B., Von Frese, R., et al., 2013. Gravity and Magnetic Exploration: Principles, Practices, and Applications. Cambridge University Press, Cambridge.

Hou, Y., Jiao, R., Yu, H., 2021. MEMS based geophones and seismometers. Sens. Actuators, A 318, 112498. https://doi.org/10.1016/j.sna.2020.112498.

INOGEO, Vectorseis ML21. datasheet. URL. http://www.inovageo.com/products/vectorseis.html.

Jewell Instruments, ASB series angular accelerometers. datasheet. URL. https://jewellinstruments.com/wp-content/uploads/Jewell_SC_Data-Sheet_ASB-Series-Angular-Accelerometer_Dec-2013.pdf.

Jewell Instruments, ASMP. datasheet. URL. https://jewellinstruments.com/products/inertial-tilt-sensors/accelerometers/asmp/.

Jewell Instruments, DMH. datasheet. URL. https://jewellinstruments.com/products/inertial-tilt-sensors/inclinometer/dmh/.

Jewell Instruments, DXI. datasheet. URL. https://jewellinstruments.com/wp-content/uploads/FI04_DXI-100-200.pdf.

Jewell Instruments, LCF. datasheet. URL. https://jewellinstruments.com/wp-content/uploads/FI14_LCF-2000.pdf.

Kasahara, J., 2002. Tides, earthquakes, and volcanoes. Science 297 (5580), 348–349. https://doi.org/10.1126/science.1074601.

Kistler. Model 8838 angular accelerometers. datasheet. URL. https://www.kistler.com/files/document/000-271e.pdf.

Krishnamoorthy, U., Carr, D.W., Bogart, G.R., et al., 2007. In-plane nano-g accelerometer based on an optical resonant detection system. In: TRANSDUCERS 2007-2007 International Solid-State Sensors, Actuators and Microsystems Conference, pp. 1195–1198. https://doi.org/10.1109/SENSOR.2007.4300350.

Krishnamoorthy, U., Olsson Iii, R.H., Bogart, G.R., et al., 2008. In-plane MEMS-based nano-g accelerometer with sub-wavelength optical resonant sensor. Sens. Actuators, A 145, 283–290. https://doi.org/10.1016/j.sna.2008.03.017.

Krishnan, G., Kshirsagar, C.U., Ananthasuresh, G.K., et al., 2007. Micromachined high-resolution accelerometers. J. Indian Inst. Sci. 87 (3), 333–361.

Laine, J., Mougenot, D., 2014. A high-sensitivity MEMS-based accelerometer. Lead. Edge 33 (11), 1234–1242. https://doi.org/10.1190/tle33111234.1.

Lei, C., Sun, X.C., Zhou, Y., 2018. Noise analysis and improvement of a micro-electro-mechanical-systems fluxgate sensor. Measurement 122, 1–5. https://doi.org/10.1016/j.measurement.2018.03.007.

Leonov, A.V., Malykh, A.A., Mordkovich, V.N., et al., 2016. A silicon field-effect hall sensor with an extended operating temperature range. Instrum. Exp. Tech. 59 (5), 724–727. https://doi.org/10.1134/S0020441216050109.

Li, B., Zhang, H., Zhong, J., et al., 2016. A mode localization based resonant MEMS tilt sensor with a linear measurement range of 360. In: 2016 IEEE 29th International Conference on Micro Electro Mechanical Systems (MEMS), pp. 938–941. https://doi.org/10.1109/MEMSYS.2016.7421786.

Li, J., Fang, J., Du, M., et al., 2013. Analysis and fabrication of a novel MEMS pendulum angular accelerometer with electrostatic actuator feedback. Microsyst. Technol. 19 (1), 9–16. https://doi.org/10.1007/s00542-012-1630-x.

Littler, I.C.M., Gray, M.B., Lam, T.T.Y., et al., 2010. Optical-fiber accelerometer array: nano-g infrasonic operation in a passive 100 km loop. IEEE Sensor. J. 10 (6), 1117–1124. https://doi.org/10.1109/JSEN.2009.2039128.

Liu, C.H., Kenny, T.W., 2001. A high-precision, wide-bandwidth micromachined tunneling accelerometer. J. Microelectromech. Syst. 10 (3), 425–433. https://doi.org/10.1109/84.946800.

Liu, H.F., Pike, W.T., Dou, G.B., 2016. A seesaw-lever force-balancing suspension design for space and terrestrial gravity-gradient sensing. J. Appl. Phys. 119 (12), 124508. https://doi.org/10.1063/1.4944709.

Liu, H.F., Pike, W.T., 2016. A micromachined angular-acceleration sensor for geophysical applications. Appl. Phys. Lett. 109 (17), 173506. https://doi.org/10.1063/1.4966547.

Liu, H.F., Pike, W.T., Dou, G.B., 2014. Design, fabrication and characterization of a micro-machined gravity gradiometer suspension. In: 2014 IEEE SENSORS, pp. 1611–1614. https://doi.org/10.1109/ICSENS.2014.6985327.

Lognonné, P., Banerdt, W.B., Giardini, D., et al., 2019. SEIS: insight's seismic experiment for internal structure of Mars. Space Sci. Rev. 215 (1). https://doi.org/10.1007/s11214-018-0574-6.

Loh, N.C., Schmidt, M.A., Manalis, S.R., 2002. Sub-10 cm/sup 3/interferometric accelerometer with nano-g resolution. J. Microelectromech. Syst. 11 (3), 182–187. https://doi.org/10.1109/JMEMS.2002.1007396.

Lu, Q.B., Bai, J., Wang, K.W., et al., 2017. Design, optimization, and realization of a high-performance MOEMS accelerometer from a double-device-layer SOI wafer. J. Microelectromech. Syst. 26 (4), 859–869. https://doi.org/10.1109/JMEMS.2017.2693341.

Luczak, S., Oleksiuk, W., Bodnicki, M., 2006. Sensing tilt with MEMS accelerometers. IEEE Sensor. J. 6 (6), 1669–1675. https://doi.org/10.1109/JSEN.2006.881433.

Marocco, G., Middlemiss, R., Prasad, A., et al., 2019. MEMS gradiometers for attitude determination on cubesats. In: 33rd Annual AIAA/USU Conference on Small Satellites, pp. 1–4.

Merchant, B.J., 2009. MEMS applications in seismology. In: Seismic Instrumentation Technology Symposium. Sandia National Laboratories.

Metcalfe, M., 2014. Applications of cavity optomechanics. Appl. Phys. Rev. 1 (3), 031105. https://doi.org/10.1063/1.4896029.

Michelena, M.D., 2013. Commercial off-the-shelf GMR based sensor on board Optos Picosatellite. In: Giant Magnetoresistance (GMR) Sensors. Springer, Berlin, pp. 181–210.

Middlemiss, R.P., Samarelli, A., Paul, D.J., et al., 2016. Measurement of the Earth tides with a MEMS gravimeter. Nature 531 (7596), 614–617. https://doi.org/10.1038/nature17397.

Milligan, D.J., Homeijer, B.D., Walmsley, R.G., 2011. An ultra-low noise MEMS accelerometer for seismic imaging. In: 2011 IEEE SENSORS, pp. 1281–1284. https://doi.org/10.1109/ICSENS.2011.6127185.

Min, Y.J., Kwon, C.K., Kim, H.K., et al., 2011. A CMOS magnetic Hall sensor using a switched biasing amplifier. IEEE Sensor. J. 12 (5), 1195–1196. https://doi.org/

10.1109/JSEN.2011.2169055.

MTMicrosystems, MSV3000-2. datasheet. URL. http://www.mtmems.com/en/product_view.asp?id=82.

MultiDimensionTechnology, TMR9112. datasheet URL. http://www.dowaytech.com/en/sensor/magnetic_field_sensors.html.

Murata, SCA103T-D04, datasheet. URL https://www. murata. com/products/productdetail?partno=SCA103T-D04.

Mustafazade, A., Pandit, M., Zhao, C., et al., 2020. A vibrating beam MEMS accelerometer for gravity and seismic measurements. Sci. Rep. 10 (1), 1–8. https://doi.org/10.1038/s41598-020-67046-x.

Novotný, D., Petrucha, V., Janošek, M., 2018. A digitally compensated AMR magnetometer. IEEE Trans. Magn. 55 (1), 1–5. https://doi.org/10.1109/TMAG.2018.2873235.

O'Brien, G.J., Monk, D.J., Najafi, K., 2003. Angular accelerometer with dual anchor support. IEEE TRANSDUCERS'03 - 12th international conference on solid-state sensors. Actuators Microsyst. 2, 1371–1374.

Pandit, M., Sobreviela, G., Pili, C., et al., 2021. A 10 nano-G/RT-hz resonant MEMS accelerometer employing anti-aliasing control. In: 2021 IEEE International Symposium on Inertial Sensors and Systems (INERTIAL), pp. 1–4. https://doi.org/10.1109/INERTIAL51137.2021.9430455.

PCB Piezotronics, Model 626A04. datasheet. URL. http://www.pcb.com/products.aspx?m=626A04.

Phan, K.L., Mauritz, A., Homburg, F.G.A., 2008. A novel elastomer-based magnetoresistive accelerometer. Sens. Actuators, A 145, 109–115. https://doi.org/10.1016/j.sna.2007.10.055.

Pike, W.T., Calcutt, S., Standley, I.M., et al., 2016. A silicon seismic package (SSP) for planetary geophysics. Lunar Planet. Sci. conf. 2081.

Pike, W.T., Delahunty, A.K., Mukherjee, A., et al., 2014. A self-levelling nano-g silicon seismometer. In: SENSORS, 2014 IEEE, pp. 1599–1602. https://doi.org/10.1109/ICSENS.2014.6985324.

Pike, W.T., Standley, I.M., Calcutt, S.B., et al., 2018. A broad-band silicon microseismometer with 0.25 NG/rtHz performance. In: 2018 IEEE Micro Electro Mechanical Systems (MEMS), pp. 113–116. https://doi.org/10.1109/MEMSYS.2018.8346496.

Pike, W.T., Standley, I.M., Karl, W.J., et al., 2009. Design, fabrication and testing of a micromachined seismometer with NANO-G resolution. In: IEEE TRANSDUCERS 2009 - International Solid-State Sensors, Actuators and Microsystems Conference, pp. 668–671. https://doi.org/10.1109/SENSOR.2009.5285413.

Projetti, M., Vancauwenberghe, O., Paulson, H., et al., 2014. Development of a MEMS rotation sensor for oilfield applications. In: 2014 IEEE SENSORS, pp. 1595–1598. https://doi.org/10.1109/ICSENS.2014.6985323.

Qu, Z., Ouyang, H., Liu, H.F., et al., 2022. 2.4 ng/rthz low-noise fiber-optic mems seismic accelerometer. Opt Lett. 47 (3), 718–721. https://doi.org/10.1364/OL.443236.

Rao, K., Liu, H.F., Wei, X.L., et al., 2020. A high-resolution area-change-based capacitive MEMS tilt sensor. Sens. Actuators, A 313, 112191. https://doi.org/10.1016/j.sna.2020.112191.

Ripka, P., 2008. Improving the accuracy of magnetic sensors. Sensors 45–60. Berlin: Springer.

Ripka, P., 2021. Magnetic Sensors and Magnetometers. Artech house, Boston.

Silicon Audio, 203-60, datasheet. URL: siaudioseismic.com/wp-content/uploads/2020/12/AGU_2019_Flyer_213P_203V.pdf.

STMicroelectronics, L6671. datasheet. URL. http://pdf.datasheetcatalog.com/datasheet/stmicroelectronics/8525.pdf.

Takahashi, H., Kan, T., Nakai, A., et al., 2019. Highly sensitive and low-crosstalk angular acceleration sensor using mirror-symmetric liquid ring channels and MEMS piezoresistive cantilevers. Sens. Actuators, A 287, 39–47. https://doi.org/10.1016/j.sna.2019.01.006.

Tang, S.H., Liu, H.F., Yan, S.T., et al., 2019. A high-sensitivity MEMS gravimeter with a large dynamic range. Microsyst. Nanoeng. 5 (1), 1–11. https://doi.org/10.1038/s41378-019-0089-7.

US Patent US6666092B2, Zarabadi, S.R., Jay, I.D., Johnson, J.D., Christenson, J.C., Noll, T.A., 2003. Angular Accelerometer Having Balanced Inertia Mass. URL: https://patents.google.com/patent/US6666092B2/en.

US Patent US20030047002A1, Arms, S.W., Townsend, C.P., 2003. MEMS Based Angular Accelerometer. URL: https://patents.google.com/patent/US20030047002A1/en.

Wang, B., Yu, L., Deng, Z., et al., 2016. A particle filter-based matching algorithm with gravity sample vector for underwater gravity aided navigation. IEEE/ASME Trans. Mechatron. 21 (3), 1399–1408. https://doi.org/10.1109/TMECH.2016.2519925.

Wang, C., Chen, F., Wang, Y., et al., 2020. Micromachined accelerometers with sub-μg/√Hz noise floor: a review. Sensors 20 (14), 4054. https://doi.org/10.3390/s20144054.

Wang, Q., Yan, S.T., Xu, Q.W., et al., 2019. A universal high-sensitivity area-variation capacitive displacement transducer (CDT) based on fringe effect. IEEE Access 7, 153650–153659. https://doi.org/10.1109/ACCESS.2019.2947570.

Wang, S., Wei, X.L., Weng, Y., et al., 2018. A novel single-Axis MEMS tilt sensor with a high sensitivity in the measurement range from 0◦ to 360. Sensors 18 (2), 346. https://doi.org/10.3390/s18020346.

Wang, Y., Song, X.X., Li, F.Z., et al., 2021. A resonant Lorentz-force magnetometer featuring slotted double-ended tuning fork capable of operating in a bias magnetic field. J. Microelectromech. Syst. 30 (6), 958–967. https://doi.org/10.1109/JMEMS.2021.3113769.

William, L., 2007. Fundamentals of Geophysics. Cambridge University Press, Cambridge.

Wu, W.J., Liu, D.D., Liu, H.F., et al., 2020. Measurement of tidal tilt by a micromechanical inertial sensor employing quasi-zero-stiffness mechanism. J. Microelectromech. Syst. 29 (5), 1322–1331. https://doi.org/10.1109/JMEMS.2020.3001928.

Xu, X.C., Wang, Q., Wang, L.J., et al., 2021. On the air buoyancy effect in MEMS-based gravity sensors for high resolution gravity measurements. IEEE Sensor. J. 21 (20), 22480–22488. https://doi.org/10.1109/JSEN.2021.3106667.

Yang, S., Zhang, J., 2021. Current progress of magnetoresistance sensors. Chemosensors 9 (8), 211. https://doi.org/10.3390/chemosensors9080211.

Yazdi, N., Ayazi, F., Najafi, K., 1998. Micromachined inertial sensors. Proc. IEEE 86 (8), 1640–1659. https://doi.org/10.1109/5.704269.

Zhang, H., Wei, X., Ding, Y., et al., 2019. A low noise capacitive MEMS accelerometer with anti-spring structure. Sens. Actuators, A 296, 79–86. https://doi.org/10.1016/j.sna.2019.06.051.

Zhou, F., Bao, Y., Madugani, R., et al., 2021. Broadband thermomechanically limited sensing with an optomechanical accelerometer. Optica 8 (3), 350–356. https://doi.org/10.1364/OPTICA.413117.

Zou, X.D., Seshia, A.A., 2015. A high-resolution resonant MEMS accelerometer. In: 2015 IEEE Transducers-2015 - 18th International Conference on Solid-State Sensors, Actuators and Microsystems, pp. 1247–1250. https://doi.org/10.1109/TRANSDUCERS.2015.7181156.

Zou, X.D., Thiruvenkatanathan, P., Seshia, A.A., 2014. A high-resolution micro-electro-mechanical resonant tilt sensor. Sens. Actuators, A 220, 168–177. https://doi.org/10.1109/FCS.2012.6243702.